Mapping landscape suitability for thinning to reduce evapotranspiration and enhance groundwater recharge in semi-arid ponderosa pine forests

Ryan E Lima[a,*], Neha Gupta[b], Travis Zalesky[b], Temuulen Tsagaan Sankey[a], Abraham E Springer[a], Patrick D. Broxton[b], Katharine Jacobs[b]

[a] *Northern Arizona University,*

[b] *University of Arizona,*

Abstract

Literature on the relationship between forest thinning and water yield was used to develop suitability criteria to map where forest treatment is most likely to enhance groundwater recharge across the ponderosa pine (*Pinus ponderosa*) forests of Arizona. Recharge in ponderosa pine forests is ephemeral and focused in periods of snowmelt and locations of enhanced permeability when soil moisture exceeds threshold levels. Our approach combines thematic maps of criteria such as fraction of precipitation as snow, slope, aspect, landscape morphology, forest basal area, canopy cover, lineament density, lithology, and hydrologic soil type into a GIS-Multi-Criteria Decision Analysis. Thematic layers were grouped into indices and suitability was determined through a weighted sum model of variables and indices. Approximately 10% (182,000 hectares) of the 1.8 million *ha* of ponderosa pine forests across western and northern Arizona were found to be highly suitable for groundwater recharge enhancement from forest thinning. This study finds that much of the area where thinning is already planned for the purpose of restoring other ecosystem services may also improve groundwater management in a state facing serious groundwater declines. This GIS-based approach enables hydrologically informed and spatially targeted forest management in semi-arid landscapes from catchment to regional scales.

Keywords: Suitability mapping, Forest thinning, Water Resources, Groundwater recharge, Potential Recharge Zones, GIS-MCDA, WSM

1. Introduction

Warming associated with anthropogenic climate change has led to a doubling in the frequency of extreme hydroclimate events in the Colorado River Basin since 2010, including droughts, heatwaves, and floods [1]. Since 2000, the Colorado River Basin has experienced a historic drought [2, 3]. Over this time period, streamflow in the Colorado River has declined by 19% (3.6E9 m^3) relative to the 1906-1999 average (18.7E10 m^3); [4, 5]. Rapid population growth in the Southwestern US, including Arizona, is increasing the demands on already strained water supplies in the State. Reductions in streamflow have increased reliance on groundwater pumping, resulting in groundwater declines across Arizona [6]. Analyses of regional gravity data have suggested that the rate of groundwater loss in the Colorado River Basin may far exceed the depletion rate of Lake Powell and Lake Mead and that groundwater may account for a more significant portion of water use than previously anticipated [7].

*Corresponding author
Email address: ryan.lima@nau.edu (Ryan E Lima)

Warming temperatures have tripled the frequency and quadrupled the size of wildfires since 2000 [8]. The risk of catastrophic wildfires is increasing in Western forests–an emerging driver of runoff change that will increase the impact on the water supply [3]. Forest structure in Northern Arizona has changed significantly post-Euro-American settlement. Many forests are overstocked relative to pre-settlement conditions due to grazing, logging, and wildfire exclusion [9, 10]. These changes have increased the risk of catastrophic wildfires [11] post-fire flooding, and debris flows [12]. Rising temperatures and droughts have contributed to extensive tree mortality from disease and insect infestation, making forested areas more vulnerable to wildfires and altering natural fire regimes, leading to hotter and more destructive wildfires [13, 14].

Forest treatments such as mechanical thinning and prescribed burning can reduce the risk of catastrophic wildfires and alter forests' hydrologic cycles [11, 15]. For example, forest thinning in Arizona has been associated with increased snow cover days [16, 17, 18], greater soil moisture [19, 20], and greater forest canopy moisture [21].

Numerous studies have linked forest treatments to increased water yields in semi-arid forests and have emphasized the role of forest thinning in improving hydrologic services and increasing water availability [22, 23, 24, 25, 26, 27, 28, 29, 30, 31, 32]. While the connection between forest treatment and water yield is well documented, the response of forests to treatments is complex and non-linear and differs across forest types, with treatment level, and along aspect and elevational gradients [15, 33, 26, 32, 34].

Regardless of the potential for increased water yield, the enhancement of groundwater recharge rarely, if ever, ranks among the primary motivations for forest treatment, even among projects with the stated goal of improving watershed health [35, 36, 11, 10, 37]. Responses from surveys of public willingness to pay for forest restoration to enhance groundwater recharge were the lowest among the environmental services discussed in the study, behind critical habitat protections, surface water quality improvements, and the preservation of cultural values[38, 39]. This suggests that groundwater recharge may be considered the least valued among other hydrologic services when considered as stand-alone services and may indicate that the general public is unaware of the complex interdependence between groundwater and surface water [38]. Groundwater is difficult to measure and visualize, so it is often undervalued and misunderstood [40, 41].

Forest health and water security are intimately linked. About 66% of the water supply in 11 western states comes from forested lands [42]. Despite this, land, surface water, and groundwater are still managed separately. The Western Water Network (WWN) identified the need to promote better collaboration between researchers, managers, educators, industry, and stakeholders across the American West [43].

This study uses an ecohydrological lens to link insights from multiple fields to examine forest restoration to groundwater recharge enhancement, and aims to identify potential recharge zones. Specifically, we demonstrate a suitability mapping approach using multi-criteria decision analysis (MCDA) to identify areas where forest thinning may enhance recharge as an additional benefit. Suitability maps like these may complement (or supplement) existing frameworks for jointly prioritizing landscape-scale forest management and managing lands and water.

MCDA has long been used in forest management for strategic (long-term, organizational) and tactical (annual) planning [44, 45]. MCDA in combination with GIS, hereafter GIS-MCDA, is a methodology that combines geographical data and value judgments to support decision-making [46]. Suitability mapping, particularly GIS-MCDA, has been widely used to map potential recharge zones and areas suitable for Managed Aquifer Recharge (MAR)[47, 48, 49, 50]. However, this study is the first to examine where forest thinning may be sited to enhance recharge at a landscape scale.

1.1. Study Area

Our study area includes all of the HUC8 (Hydrologic Unit Code 8) watersheds of Arizona, extending into 5 other U.S. states. The portions of HUC8 watersheds in Mexico were excluded due to a lack of data. However, within that study area, we focus on the ponderosa pine (PIPO) woodland type, which covers approximately 1.8 million *ha* (1,835,530.65) of this area, comprising 28% of the forested area within its bounds. Most PIPO forest is found along the Mogollon Rim, around the San Francisco Peaks, and on the Kaibab Plateau–all within the Colorado Plateau physiographic region at elevations between 2000 *m* and 2400 *m*. Smaller isolated patches of PIPO forest can be found on mountain ranges and plateaus throughout Arizona at similar elevations (Figure 1).

The Mogollon Rim is a topographic feature forming the southern edge of the Colorado Plateau. It contains most of the state's PIPO forests and has been identified as an essential groundwater recharge area for regional aquifers [51]. Of the estimated 2.1 billion m^3 (174,000 acre-feet) of precipitation that falls on the Mogollon Rim annually, about 8% is estimated to recharge the regional groundwater aquifers[51] Similarly, The Kaibab Plateau, an uplifted region north of the Grand Canyon with large stands of PIPO, is a critically important recharge area for springs in the Grand Canyon which provide the sole source of drinking water for over 6 million annual visitors and the residents of Grand Canyon National Park[52]. The Kaibab Plateau lacks perennial surface streams and is drained rapidly by sinkholes, faults, and fractures or more slowly through diffuse infiltration with little streamflow leaving the plateau [53, 54].

Most of the PIPO forests within Arizona are within the Kaibab, Coconino, Apache-Sitgreaves, Tonto National Forests, The Fort Apache Reservation, and Navajo Nation. Precipitation in Arizona is bi-modal, with wet winters and a late-summer monsoon season. As much as 60% of precipitation at elevations above 2000 *m* comes in the form of snow, and snow is responsible for 80 - 95% of streamflow and much of the recharge [55, 56, 57]. Therefore, this research focuses on high-elevation (>= 2000 *m*) PIPO forests, which receive a high proportion of annual precipitation as snow. Of the 1.8 million *ha* of PIPO forests in our study area, about 43% or 790,000 *ha* are underlain by lithologies that may include karst or pseudo-karst features, including carbonates (24%), evaporates (6%), and fractured volcanics (13%). These areas merit extra attention due to enhanced infiltration potential through fractures, faults, lava tubes, or sinkholes.

1.2. Literature Review and Criteria

This research aims to identify areas where mechanical thinning is most likely to enhance groundwater recharge. We based our suitability criteria on literature primarily from regional studies, as they likely provide usful information about hydrologic response to thinning in Arizona's forests [58]. Landscape-scale forest restoration efforts have been planned or implemented across much of Arizona. For example, the Four Forest Restoration Initiative (4FRI) includes a goal of restoring over 1 million hectares of Arizona's forests [59]. A synthesis study of 4FRI treatments found that thinned and burned forests have significantly greater total ecosystem moisture and are thus more resilient to drought and wildfire [20, 21]. Thinned forests also have more snow and soil moisture [60, 19].

Snow and its persistence appear particularly important for recharge in Arizona's semi-arid and high-elevation conifer forests. An analysis of groundwater coming from springs along the Mogollon rim found a strong relationship between snow persistence and the duration of spring discharge [61]. Isotopic groundwater analyses have revealed that Northern Arizona's recharge is dominated by winter precipitation from altitudes above 1500 m[56, 57, 62, 63]. Studies of plant water use have found that larger PIPO trees primarily utilize deeper soil moisture from winter precipitation, while understory vegetation and smaller trees utilize shallow soil water from monsoonal storms[64, 65].

Thinning in PIPO forests is expected to increase available water in two ways: 1) reducing transpiration of deep soil water by overstory vegetation and 2) reducing sublimation of intercepted snowfall, which could increase below canopy snow depth and persistence. Thinning in semi-arid forested watersheds can significantly alter snowmelt timing [66]. Reduced forest cover can delay snowmelt at colder sites, higher elevations, and northern aspects or advance snowmelt through increasing sub-canopy solar radiation and wind, particularly at lower elevations, southern aspects, and warmer sites [67, 66].

Total annual precipitation also appears to influence whether thinning reduces or enhances water yield at particular sites. In the Colorado River Basin, there appears to be a precipitation threshold for hydrologic responses. Below ~500 *mm* of annual precipitation, precipitation and runoff may become decoupled [33], likely because below ~500 *mm*, most precipitation is evaporated regardless of forest condition. Semi-arid

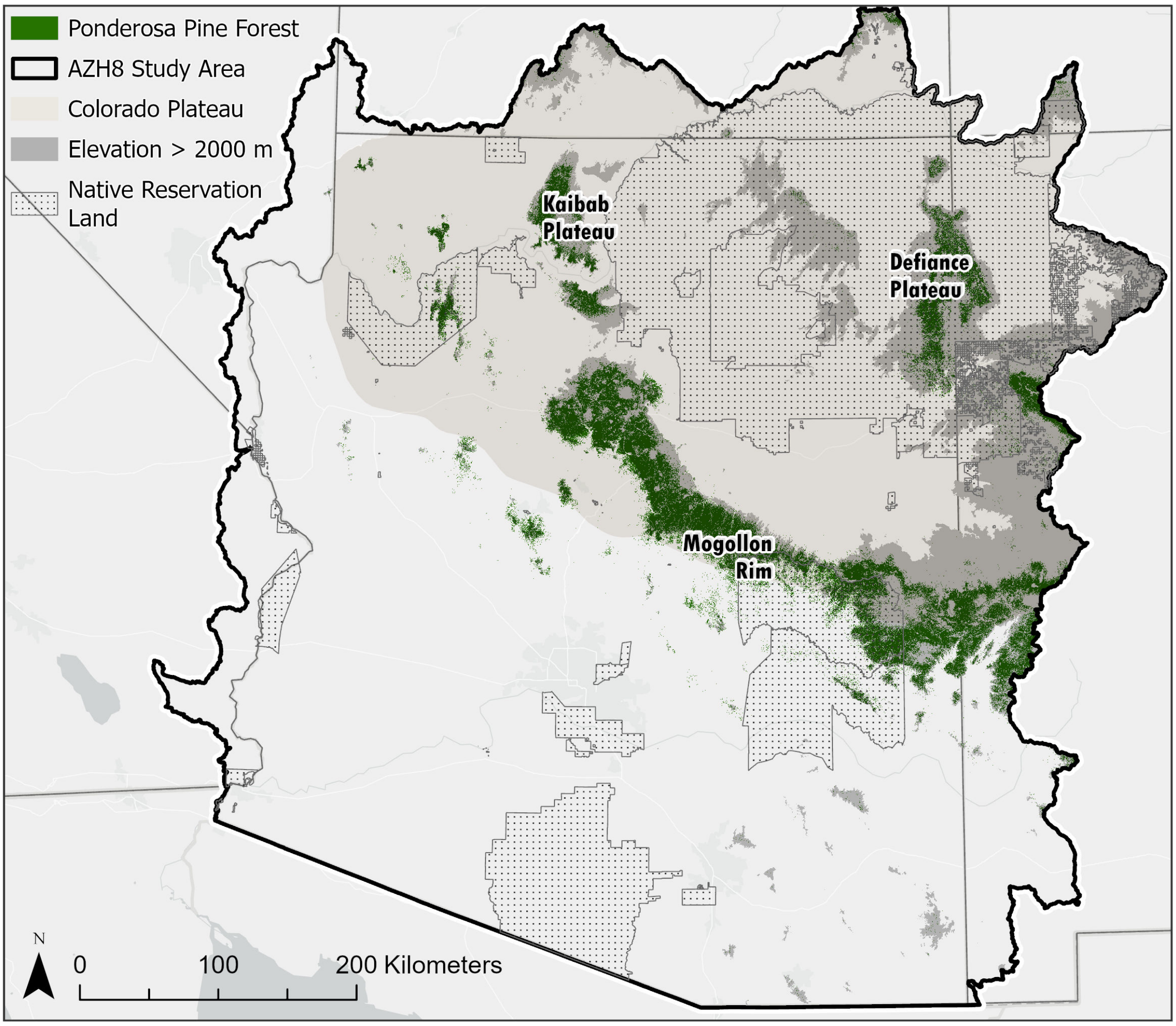

Figure 1: Study area reference map with an emphasis on high elevation (dark gray), Colorado Plateau (beige area), Native reservation land (dotted) and the distribution of PIPO-dominated forests (green) considered by this analysis.

forests with high inter-annual precipitation variability may show effects in wet years when precipitation is greater than ~500 *mm* or in snow-dominant watersheds [68, 69].

Reductions in canopy cover can reduce transpiration losses and decrease soil moisture stress [70, 60, 71, 20] or increase surface evaporation and sublimation depending on the elevation, aspect, and the amount of canopy removed [72, 73, 74]. Canopy cover between 25% and 40% appears optimal for net snow accumulation at continental mid-latitude sites [75], though this is dependent on elevation and aspect, with lower forest densities being optimal areas with shorter snowpack duration (such as low elevations) and higher forest densities being optimal for areas with longer snowpack duration [76]. UAV-based studies within the study area have shown that 24 - 35% canopy cover was optimal for snow persistence. [18, 16, 17]. However, water yield enhancement from thinning likely requires at least a 20% reduction in canopy cover [68]. Hydrologic models in northern Arizona watersheds suggest that reductions in basal area of at least 30% can increase groundwater recharge by up to 15% [30].

Research on the effect of thinning to below-ground hydrological processes in semi-arid Mediterranean forests found that sites with high antecedent soil moisture had the highest response, with drainage to deeper soil layers increasing by 50 *mm/year* relative to control sites[77]. Soil type (texture, composition, field capacity, and permeability) and topography affect soil moisture conditions. Slope, aspect, landscape convexity or concavity, and geomorphons (or landform types) such as pits, flats, hills, valleys, ridges, and hollows strongly affect the accumulation and residence time of overland flow and shallow soil water [78, 79]. In dry soils, capillary forces generally dominate over gravitational forces, and areas with higher flow accumulation and residence time are more likely to reach field capacity, leading to more percolation [80].

Another important aspect affecting recharge enhancement potential is the underlying lithology, which controls the subsurface flow of groundwater. Arizona currently lacks detailed hydrogeologic mapping. However, representative ranges of primary (matrix) permeability and porosity values for rock types are available based on 1:1,000,000 and 1:500,000 geologic mapping data[81, 82, 80]. Secondary permeability and porosity, which involve flow in faults and fractures, can be estimated by measuring the density of linear surface features, or 'lineaments,' which often correspond to underlying geologic structures [83, 84]. Lineaments have been used to identify potential groundwater supplies, and studies have found higher well yields along lineaments [84]. In some crystalline bedrock, groundwater flow occurs exclusively in faults and fractures [85, 86]. Orientations of lineaments can help determine the anisotropy of the fracture environment[85]. Caves and sinkholes (or dolines) often form along and at the intersection of faults and fractures in karst terrains [87]. Karst and pseudo-karst terrains can have enhanced infiltration potential far beyond the hydraulic conductivity of the rock matrix [88]. For example, the Edwards Aquifer in Texas was found to have permeability values that vary by up to nine orders of magnitude [89]. The presence or absence of karst or pseudo-karst in concert with lineament density is a critical criteria in our suitability analysis.

In summary, suitable sites where thinning enhances recharge would most likely occur in areas with significant snowfall, maximum annual precipitation >= 500 *mm*, higher antecedent soil moisture, NE aspects, in valleys or flat areas where a 20% reduction in canopy cover and a 30% reduction in basal area would result in a thinned canopy cover of between 25 and 35%. Suitability would be lowest in sites with minimal snowfall, SW aspects, lower elevations, ridge tops, or steep slopes, where thinning might reduce canopy cover to below 24%. Soil hydraulic conductivity, flow accumulation, and topographic metrics can reveal the areas likely to have higher antecedent soil moisture. Lithology, primary permeability and porosity, and lineament density can provide insight into where rapid subsurface infiltration is possible.

2. Methods

The MCDA-GIS suitability mapping process generally involves defining the objective, screening suitable areas, classifying thematic layers or criteria, standardizing, weighing, and sensitivity analysis [46, 45]. In this case, the objective is to determine the relative suitability of areas to achieve enhanced recharge through forest treatment. The criteria were selected based on a review of the literature in Section 1.2 . Standardization was achieved by scaling variables and final suitability on a scale of 1 - 10, from lowest to highest suitability, to facilitate straightforward interpretation. Weighting the relative contribution of 12 different variables, some likely exhibiting strong collinearity, through pairwise comparison would be complex. To address this challenge, similar variables were consildated into indices, which were subsequently weighted against each other, streamlining analysis and reducing redundancy.

2.1. Suitability Criteria

We used ArcGIS Pro 3.4.0 to create a weighted suitability model consisting of the 12 thematic data layers (Table 1). These data layers were re-scaled, weighted, and combined into four final thematic layers: (1) Snowfall fraction (SF), (2) Vegetation Density Index (VDI), (3) Soil Moisture and Infiltration Index (SMII), and (4) Subsurface Infiltration Index (SbII : Table 1) weights within and between indices were assigned using pairwise comparisons, and applied using weighted linear sums.

Table 1: Thematic Layers and Indices used for suitability mapping.

Thematic Layer	Intermediate Index	Scaled Variable	Data Layers	Source
SF	-	sSF	Snowfall Fraction	UA SnowData (800m)
VDI	-	sBA	Basal Area	TreeMap 2016 (30m)
VDI	-	sCC	Canopy Cover	NLCD 2021 (30m)
SMII	TRMI	sApt	Aspect	Derived from 1-Arcsecond DEM
SMII	TRMI	sGeo	Geomorphon	Derived from 1-Arcsecond DEM
SMII	TRMI	sSlop	Slope	Derived from 1-Arcsecond DEM
SMII	TRMI	sTPI	Topographic Position Index	Derived from 1-Arcsecond DEM
SMII	-	sSoilK	Soil Saturated Hydraulic Conductivity	ggNATSGO (30m)
SbII	-	sPo	Matrix Porosity	GLHYMPS v2
SbII	-	sPm	Matrix Permeability	GLHYMPS v2
SbII	-	sLD	Lineament Density	Derived from 1-Arcsecond DEM
SbII	-	sPK	Potential Karst or Pseudo-Karst	Karst in the United States (USGS)

2.1.1. Snowfall Fraction (SF)

Snowfall Fraction (SF) is the percent of annual precipitation that comes in the form of snow. The SF metric was created using accumulated snowfall calculated from the University of Arizona snowpack (UA Snow) data [90] by summing positive increments of snow water equivalent (SWE; to estimate snowfall) and dividing by accumulated precipitation from PRISM [91]. The UA Snow data, itself is based on the interpolation of SWE and snow depthh measurements from ground stations against a background field of snowpack estimates created using PRISM precipitation and temperature data, and importantly, it contains an algorithm that separates rainfall and snowfall based on a spatiotemporally variable rain-snow transition temperature that varies based on station whether stations record snow accumulation [92]. Note that in this study, we use the 800 m version of the UA data [93].

Snowfall is important for recharge at elevations over 2000 m in Arizona [56, 55, 57]. Snow dominance and snowmelt duration are critical factors in whether thinning enhances recharge [68, 69, 94]. Therefore, our suitability mapping prioritizes areas with more snowfall relative to rainfall (higher SF). SF was scaled linearly from 1 to 10 to create a scaled snowfall fraction (sSF) thematic layer.

2.1.2. Vegetation Density Index (VDI)

The Vegetation Density Index (VDI) is created from two data layers, canopy cover (CC) and basal area (BA).

2.1.2.1. Canopy Cover (CC).

Canopy Cover was obtained from the 2021 National Land Cover Database (NLCD), which estimates total canopy cover at a 30m resolution. CC values ranged from 0% - 86%. The variable NLCD TCC (total canopy cover) was reclassified from 1 to 10 based on suitability for thinning to enhance recharge. Forest canopy cover<= 12.5% was reclassified as equal to 1, scaling suitability linearly up to CC >= 28.75% equal to 10 (see appendix: Figure 12;Figure 11). These threshold values were determined by considering a minimum 20% reduction in CC without dropping below the pre-settlement minimum CC of 10% [95]. Studies examining the relationship between CC and snow retention in PIPO forests found that 23% to 35% is the ideal CC range for retaining snow[75, 18, 16, 17]. Areas with CC currently exceeding 28.75%, were considered ideal candidates for thinning. The scaled canopy cover (sCC) thematic layer resulting from this reclassification function was used as an input layer for further analysis.

2.1.2.2. Basal Area (BA).

We extracted BA estimates from the TreeMap 2016 [96] CONUS dataset with a resolution of 30 meters. BA was rescaled similarly to canopy cover assuming a 30% reduction required to increase water yield, and a pre-settlement estimate of between 9.2 and 18 m^2ha^{-1} for PIPO [95]. BA was therefore rescaled linearly from <= 13.14 m^2ha^{-1} equal to 1, up to >= 25.71 m^2ha^{-1} equal to 10, see appendix (Figure 11;Figure 12). The scaled basal area (sBA) layer resulting from this reclassification function was used as an input layer for further analysis.

2.1.2.3. Creation of VDI.

BA and CC are often highly correlated but represent different aspects of forest structure. Therefore, they were combined into a single index. Vegetation density index (VDI) is the weighed sum of sBA, and sCC was combined with weights of 0.6667 and 0.3333, respectively, to create the vegetation density index (VDI)(Equation 1). We used pairwise comparisons to compare the importance of the two variables and ultimately assigned a higher weight to the basal area. This reflects the fact that reductions in basal area are more likely correlated with reductions in transpiration, while canopy cover primarily affects precipitation partitioning and sub-canopy solar radiation.

$$VDI = sBA * 0.6667 + sCC * 0.3333 \tag{1}$$

2.1.3. Soil Moisture and Infiltration Index (SMII)

Soil Moisture and Infiltration Index (SMII) consists of two data layers, Soil Hydraulic Conductivity (SoilK) and Topographi Relative Moisture Index (TRMI), which includes several topographic paramters derived from a digital elevation model (DEM).

2.1.3.1. Soil Hydraulic Conductivity (SoilK).

SoilK is used to estimate the max infiltration rate of the soil profile. SoilK comes from the gridded National Soil Geographic Database produced by the USDA-NRCS. The gNATSGO Soil hydraulic conductivity layer estimates the rate at which water moves through the pores of saturated soil based on point field measurements of soil texture, structure, and porosity. Data was extracted from the gNATSGO database for the AZHUC8 study area. The depth-weighted average method was used to calculate values for soil layers from 0 - 200 *cm* for each 30 by 30 *m* pixel, using the Soil Data Development Toolbox in ArcMap 10.8.3. Values are reported in micrometers per second and broken into the standard 6 classes from very low (0.00 - 0.01) to Very High (100 - 705). These standard classes were assigned suitability values between 1 and 10 to create a scaled SoilK layer (sSoilK)(Figure 2). See Table 2 in the appendix for more details.

2.1.3.2. Topographic Relative Moisture Index (TRMI).

TRMI incorporates several topographic parameters that influence moisture dynamics, including slope gradient, aspect, relative elevation (or topographic position), and landscape convexity or concavity [78] (see appendix: Figure 15). TRMI was calculated as per [78] by reclassifying and then summing each of the input layers; slope (degrees) (1-10), slope configuration or topographic position index (TPI)(1-10) [97], geomorphon (ArcGIS Pro 3.4.0 Spatial Analyst Toolbox–Geomorphon Landform Tool) (1-20), and aspect (degrees azimuth) (1-20). The resulting TRMI values were between 4 and 60, subsequently reclassified into 10 classes with equal interval breaks to create a scaled TRMI layer (sTRMI). Additional details regarding the geomorphon layer and specific reclassification functions used for each input layer can be found in the appendix (Table 3;Table 4;Table 5).

2.1.3.3. Creation of SMII.

The Soil Moisture and Infiltration Index (SMII) represents where water accumulates on the landscape and where it is likely to infiltrate through the top 2 meters of the soil profile. This index is a weighted sum of the TRMI and SoilK (Figure 2). We prioritized moisture supply (TRMI) over infiltration (SoilK), reasoning that infiltration matters less in areas with no accumulated water to infiltrate. Hence, we applied a weight of 0.6667 to sTRMI and 0.33333 to sSoilK (Equation 2;see appendix:Figure 13).

$$SMII = sTRMI * 0.6667 + sSoilK * 0.3333 \tag{2}$$

2.1.4. Subsurface Infiltration Index (SbII)

The Subsurface Infiltration Index (SbII) was created by combining layers of Matrix Pereabolity (Pm) and Porosity (Po), Lineament Density (LD), and Potential karst of Pseudo-karst (PK).

2.1.4.1. Matrix Permeability (Pm) and Porosity (Po).

Pm and Po values were extracted from the GLobal Hydrogeology MaPS 2.0 (GLHYMPS v2) dataset [81]. Our study area contained 11,057 polygons with values for saturated log-permeability ranging from -16 to -10 and porosity values ranging from 0.01 - 0.28 (Figure 10, see appendix). The attribute values were extracted, the polygons were rasterized at a 30m resolution and then re-scaled to values (1-10). See the appendix for more details on the rescaling of Po and Pm (Table 6).

2.1.4.2. Lineament Density (LD).

Lineaments are linear or curvilinear surface features that may reflect subsurface geologic structures[83]. Lineament density(LD) is commonly used in studies evaluating potential recharge zones [98, 99, 100]. Lineaments were extracted from U.S. Geologic Survey, 2019 3D Elevation Program 1-arc-second tiles using the LINE algorithm in Catalyst 3.0.2. the process is described in detail in the appendix. The ouput of the LINE tool was exported as a shapefile and analysed using the Line Density Tool in ArcGIS Pro to calculate the density of lineaments within a circular neighborhood with a radius of $1km$, providing lineament density values between 0.001 and 5.55 km/km^2. While the presence of lineaments likely enhances the secondary Pm and Po, the absence of lineaments does not necessarily reduce overall recharge suitability. Therefore, we scaled lineament density between 5 and 10 for the thematic layer scaled lineament density (sLD) (see appendix: Figure 16); this is consistent with other GIS-MCDA studies evaluating recharge potential [50].

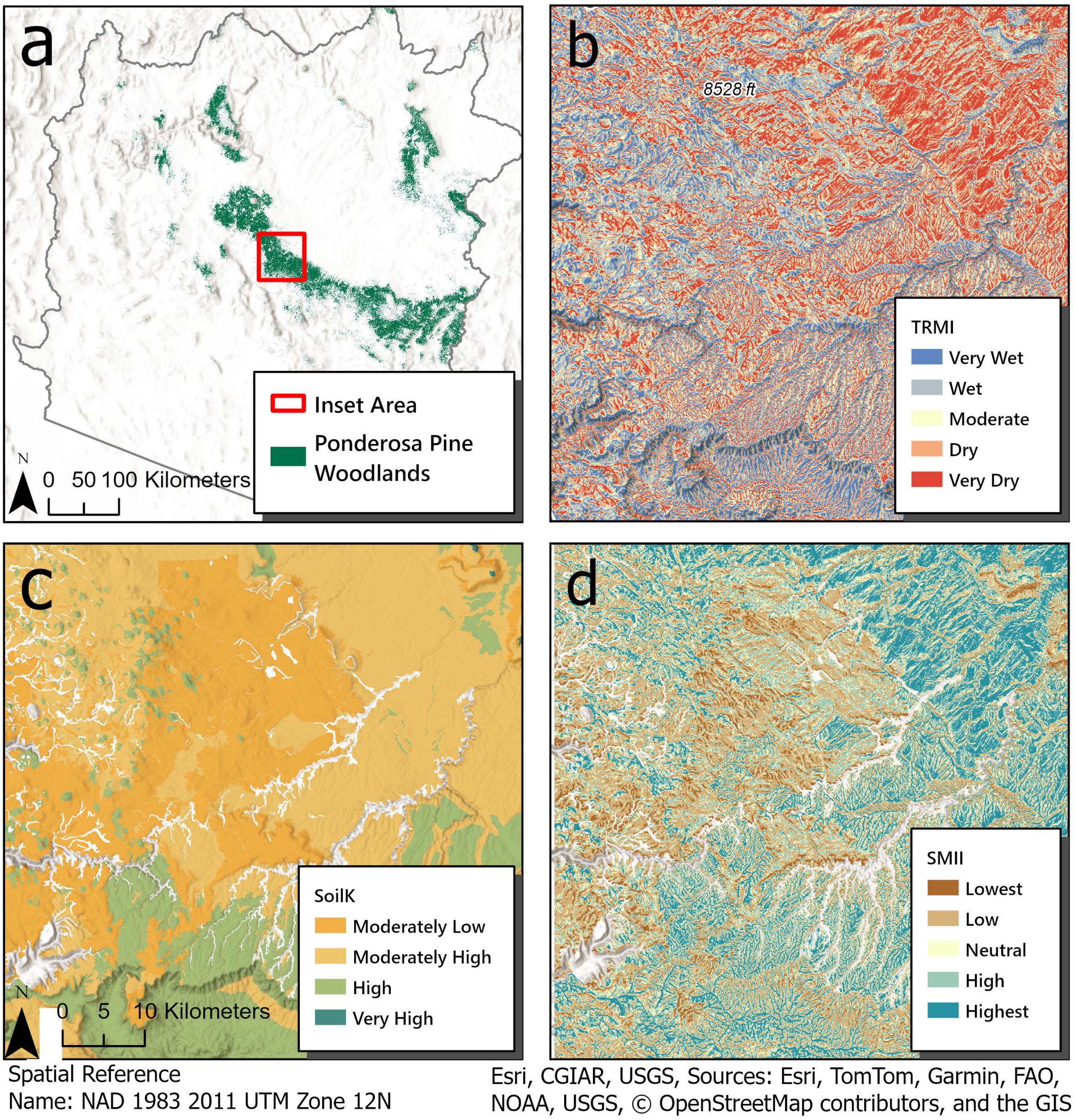

Figure 2: Panel (a) shows the zoomed-in area for panels (b), (c), and (d).Soil Moisture and Infiltration Index (SMII) (d) is composed of a weighted linear sum of the scaled Soil hydraulic Conductivity (SoilK)(c) and the scaled Topographic Relative Moisture Index (TRMI)(b).

2.1.4.3. Potential Karst or Pseudo-Karst (PK).

Shapefiles of potential karst or pseudo-karst lithology (PK) were sourced from the Karst in the United States digital map compilation and database [101]. The polygons were clipped to the AZHU8 study area and converted to a $30m$ raster, and assigned values based on their potential for enhanced recharge through faults, fractures, sinkholes, or caves. The classes were non-karst = 5 (neutral), volcanics with potential karst or pseudo-karst (such as lava tubes) = 7, evaporates at or near the surface = 8, and carbonates at or near the surface = 10, resulting in a scaled potential karst layer (sPK).(Figure 3)

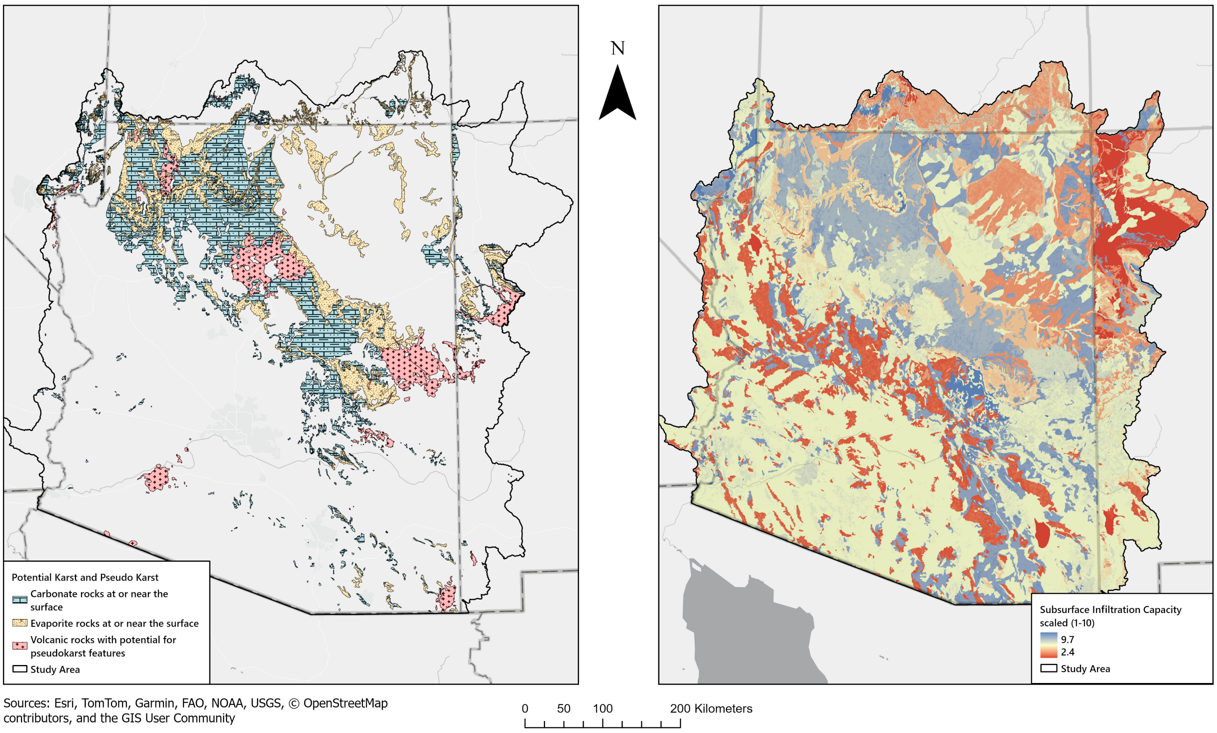

Figure 3: Potential karst or pseudo-karst (left) areas with potential karst features may have higher permeability and porosity through sinks, caves, lava tubes, voids, and fractures. Subsurface infiltration index is shown on the right, areas with high infiltration potential are in blue, while areas with low subsurface infiltration potential are in red.

2.1.4.4. Creation of SbII.

SbII is a weighted linear sum of sPm, sPo, sLD, and sPK, with weights 0.4, 0.25, 0.15, and 0.2, respectively; the equation is shown below (Equation 3)(Figure 3; see appendix: Figure 14). The SbII can be seen as an estimate of the infiltration potential of the subsurface lithology excluding soils (which are included in the SMII index). Due to the resolution of the geologic mapping that produced the GLHYMPS v2 dataset and general lack of detailed geologic mapping in much of Arizona, focused recharge in stream channels is not addressed by this index, and it can be seen as a conservative estimate of recharge potential state-wide.

$$SbII = sPm * 0.4 + sPo * 0.25 + sLD * 0.15 + sPK * 0.2 \tag{3}$$

2.2. Overall Suitability Weighting

The four final thematic layers: sSF, VDI, SMII, SbII were ranked in order of importance and assigned weights of 0.2, 0.2, 0.4, and 0.2 respectively and combined using a weighted sum resulting in the final suitability values for thinning to enhance recharge (Equation 4). The relative proportion, or percent contribution of each thematic layer to overall suitability is shown in Figure 4

$$FinalSuitability = 0.2 * sSF + 0.2 * VDI + 0.4 * SMII + 0.2 * SbII \quad (4)$$

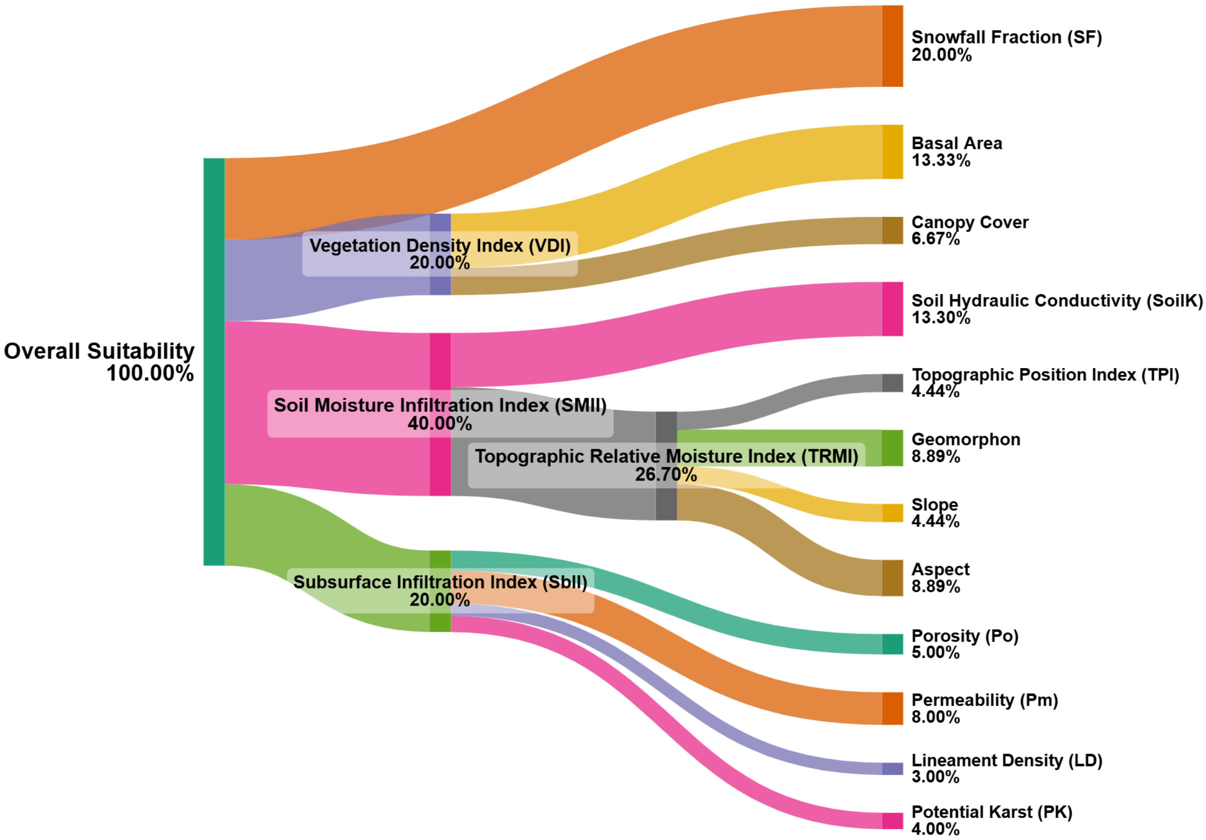

Figure 4: Sankey diagram showing the relative contribution of each thematic layer and indices to the overall suitability for thinning to enhance recharge. Note that the relative contribution of each component of each index must be multiplied by the index weight to see their relative contribution to overall suitability.

2.3. Sensitivity Analysis

A sensitivity analysis was conducted on a subset of the data using a one-at-a-time (OAT) analysis, where each parameter was systematically removed from the VDI, SMII, SbII and final suitability. Also, for each of the indices and final suitability, the applied weights were shuffled to determine the effect of differing the weights on mean pixel values and the percentage of pixels with values over 5, 6, and 7, representing areas of moderate, high, and very high suitability, respectively, for thinning to enhance recharge. Altogether, 32 different weighting simulations and 14 removal simulations were conducted on the various indices and final suitability(see appendix tables 8-14). For each index and final suitability, the resulting indices from weight shuffling and variable removal were stacked. The Coefficient of Variation (CoV), mean, range and standard deviation were calculated for all pixels (x,y) and plotted to indicate where variability in suitability numbers manifested spatially and to understand the uncertainty in index values (see appendix: Section 8.3).

3. Results

3.0.1. Overall Suitability

The study area contained 1.8 million *ha* of PIPO forest. Approximately 44% (807,000 *ha*) of the PIPO forest was deemed suitable (> 6) and about 10% (182,000 *ha)* were deemed highly suitable (>7) for thinning to enhance recharge (Figure 5; Figure 9 in appendix). The remainder of the PIPO forest is moderate suitability, low suitability, or not suitable for thinning to enhance recharge 41% (762,000 *ha*). About 48% of the area was marginally suitable or marginally unsuitable (4 - 6), and about 8% (141,000 *ha*) was found to be unsuitable for thinning to enhance recharge.

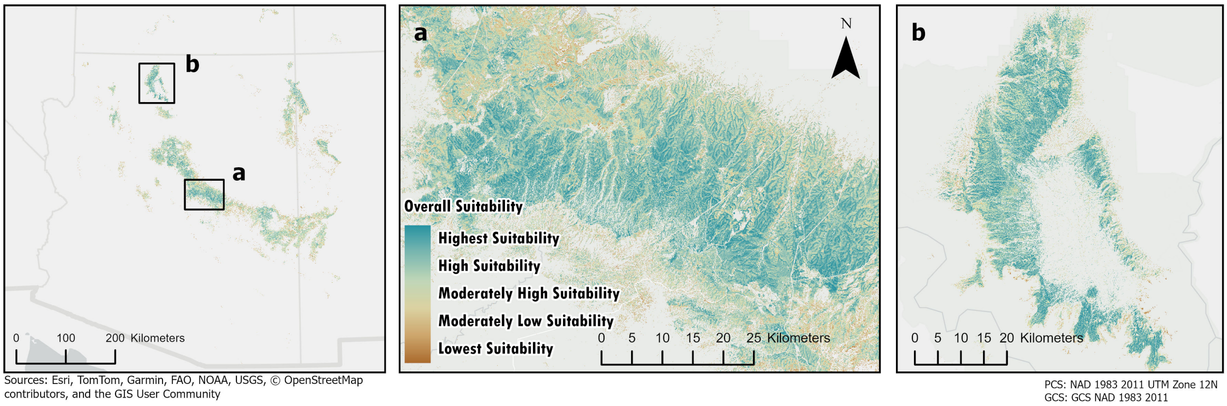

Figure 5: Suitability Map for Thinning to Enhance Groundwater Recharge

4FRI has planned (through Environmental Impact Statements) or implemented thinning on about 180,000 *ha* of PIPO forest [102]. Within those areas, about 16% or 30,000 *ha* are highly suitable for thinning to enhance groundwater recharge (or have suitability values >= 7). Within the 4FRI planning area, there are still about 540,000 ha, which are not part of areas planned for thinning in one of the two currently existing environmental impact surveys. About 12% or 65,000 ha of that area are highly suitable for thinning to enhance groundwater recharge (or have suitability values >= 7) (Figure 6). This information can help forest managers decide which areas to include in the next phase of planning and provide information on the co-benefits of thinning for recharge enhancement as well as forest health and fire risk mitigation.

Large areas of high-suitability PIPO forest can also be found on the Fort Apache Reservation along the Mogollon Rim, and in Navajo Nation on the Defiance Plateau and in the Chuska Mountains, which are located to the north of the Mogollon Rim near the border between Arizona and New Mexico(Figure 7). Groundwater security is particularly important in native communities. Over 70,000 members of the Navajo Nation lack running water and haul water, often from wells [103, 104].

3.0.2. Sensitivity Analysis Results

3.0.2.1. VDI Sensitivity.

Shuffling the weights of sCC and sBA resulted in a relatively small (0.3) change in the mean value, of VDI, and a relatively small change in the percent of pixels which were highly suitable (>7). Suggesting that either approach likely would not change the results of the final suitability very much. There were some marginal changes though the percent of moderately suitable (>5) and moderately high suitable pixels (>6). Some differences are also apparent when looking at the pixel-wisee variability, where large patches of forest have relatively high CoV values. After taking a closer look, these are areas with high canopy cover but low basal area, this is reassuring because it shows that these two variables are non-redundant (see appendix:Table 8; Figure 17). The OAT removal of each variable in VDI resulting in slightly larger changes to overall suitability than the weight swapping, removing canopy cover increased the mean value, suggesting it might be the limiting factor(see appendix:Figure 18; Table 9).

3.0.2.2. SMII Sensitivity.

SMII values increased when sTRMI had a lower weight relative to sSoilK and when sTRMI was removed. This suggests that sTRMI is limiting suitability in areas where there is high soil permeability. The inclusion

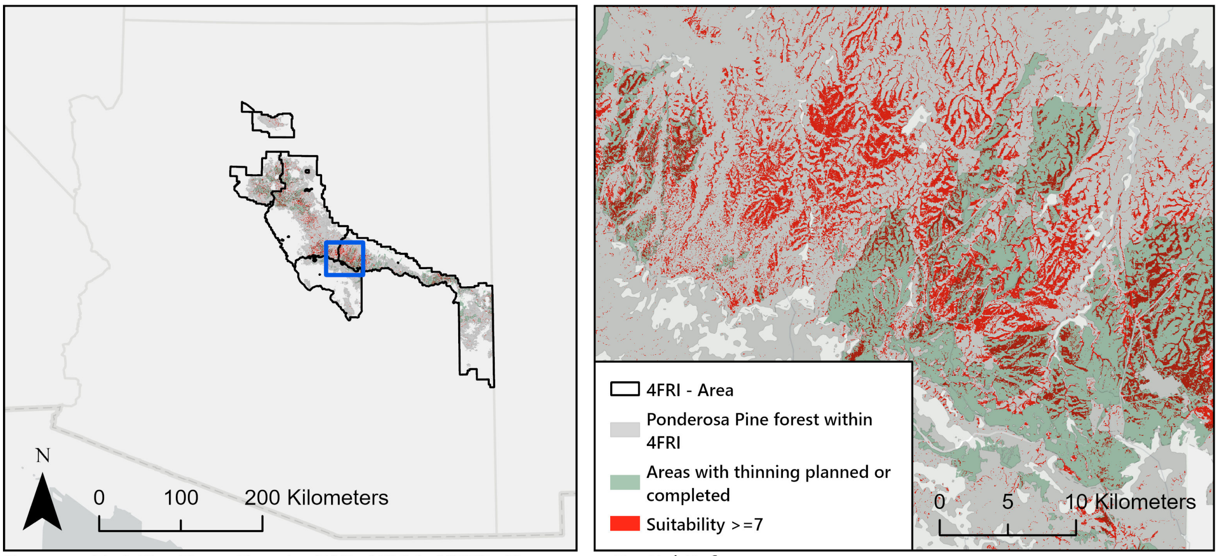

Sources: Esri, TomTom, Garmin, FAO, NOAA, USGS, © OpenStreetMap contributors, and the GIS User Community

Spatial Reference
Name: NAD 1983 2011 UTM Zone 12N

Figure 6: Map showing the Four Forest Restoration Initiative (4FRI) area. Suitability values greater than 7 are highlighted in red. Areas where thinning has been planned or completed are shown in green, and areas of PIPO forest that have not yet been included in an environmental impact studies are shown in grey.

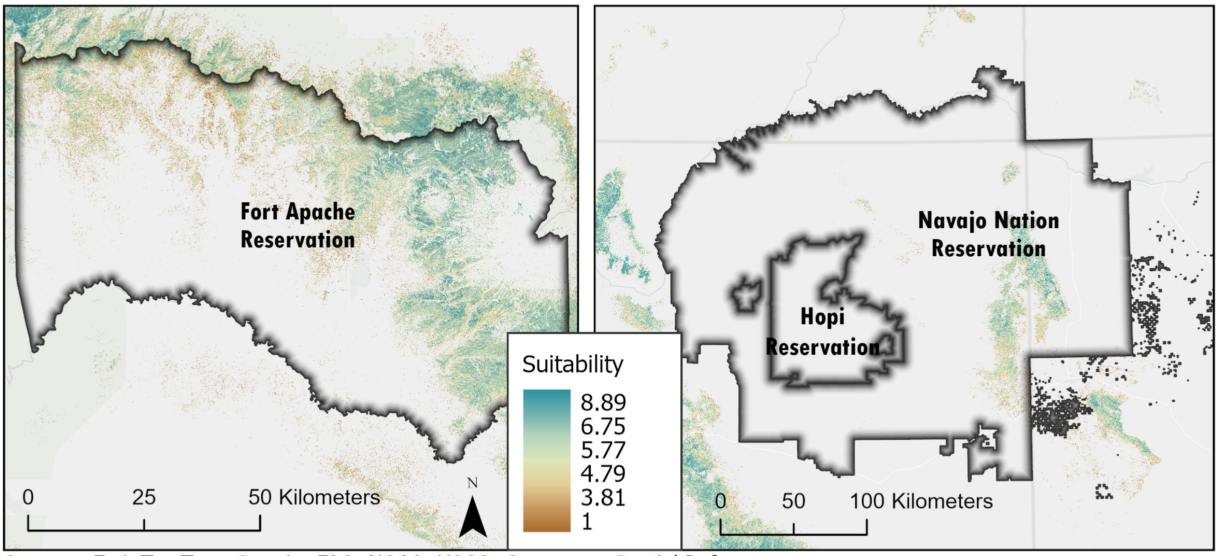

Sources: Esri, TomTom, Garmin, FAO, NOAA, USGS, © OpenStreetMap contributors, and the GIS User Community

Spatial Reference
Name: NAD 1983 2011 UTM Zone 12N

Figure 7: Suitability of thinning to enhance recharge in the Fort Apache Reservation (left) and Navajo Nation (right).

of TRMI is an important aspect of recharge potential, and it is acceptable that its addition reduces suitability in some places (See appendix: Table 10; Figure 19; Table 11; Figure 20).

3.0.2.3. SbII Sensitivity.

There were 24 possible weighting combinations for SbII, because sLD and sPK were scaled 5-10 nearly all of the area had values >5. However, lower mean values and a lower percentage of high suitability pixels (>7) were observed when sPo was weighted heavily. The same pattern is found when sPo was removed–higher mean and high suitability values. Suggesting the sPo is the limiting factor. sLD also appears to be a factor limiting suitability as shown by the removal of that variable and resulting lower mean suitability values. High SbII then appears to be driven permeability and Karst lithology, which is what we would expect. The variability between runs shows that these variables are non-redundant (see appendix: Table 12; Figure 21; Table 13; Figure 22).

3.0.2.4. Sensitivity of Overall Suitability.

Variability, or uncertainty in final suitability values was systematically examined by removing variables OAT, and shuffling weights (see appendix: Table 14; Figure 23; Table 15; Figure 24). The max pixel-wise CoV when swapping weights was about 0.5 or a 50% change in final suitability values. The high CoV values are mostly found in square blocks, which correspond to the SF raster's 800m pixels before resampling, suggesting that high variability is being driven by the sSF raster primarily; their scattered distribution suggests that they may be related to noise in the precipitation data. Otherwise, variability appears high along major river channels, likely due to edge effects and having no data for some valley bottoms (Figure 8).

4. Discussion and Conclusion

The sensitivity analysis showed that results after weighting changes and variable removal were relatively consistent and interpretable. Changes in suitability when removing or re-weighting variables are expected if variables are non-redundant. Most of the changes in suitability values for all indices could be explained and are not at odds with the reviewed literature. The overall mean pixel-wise range for suitability values was 1.4; therefore, the suitability values for any given spot are likely uncertain by +/—1.4. Modeling or field studies could help reduce the overall uncertainty.

This research demonstrates a novel application of GIS-MCDA for mapping areas where forest thinning could enhance groundwater recharge. The methodology here is adaptable and could be implemented in other semi-arid forested regions. More work is needed to validate suitability maps using process-based hydrologic models.

Forest thinning is already planned in over 1 million *ha* of Arizona's PIPO forest. Thinning is intended to reduce the risk of catastrophic wildfires, protect forest resources, enhance surface water provisioning, and improve habitat. However, we have also demonstrated that thinning will likely enhance groundwater recharge in much of the PIPO forest. This important co-benefit may increase stakeholder buy-in and strengthen justification for management actions.

As water managers across the state struggle to secure new water supplies to meet the demands of population growth and maintain the agricultural economy, insecurity in supplies from the Colorado River means that more and more water users are turning to groundwater to fill the gap. Increased interest in thinning to enhance recharge could encourage land managers to speed-up the pace of restoration and demonstrate the value of thinning to water managers looking to improve water supply resiliency, potentially providing an alternative funding source.

The Forest Service is mandated to manage for multiple uses; however, groundwater recharge is not currently an explicitly managed use. In 2014, the US Forest Service introduced a proposed directive that would mandate the consideration of groundwater resources within its activities. However, push-back from stakeholders and state water management agencies led to the withdrawal of this directive, with the Forest Service vowing

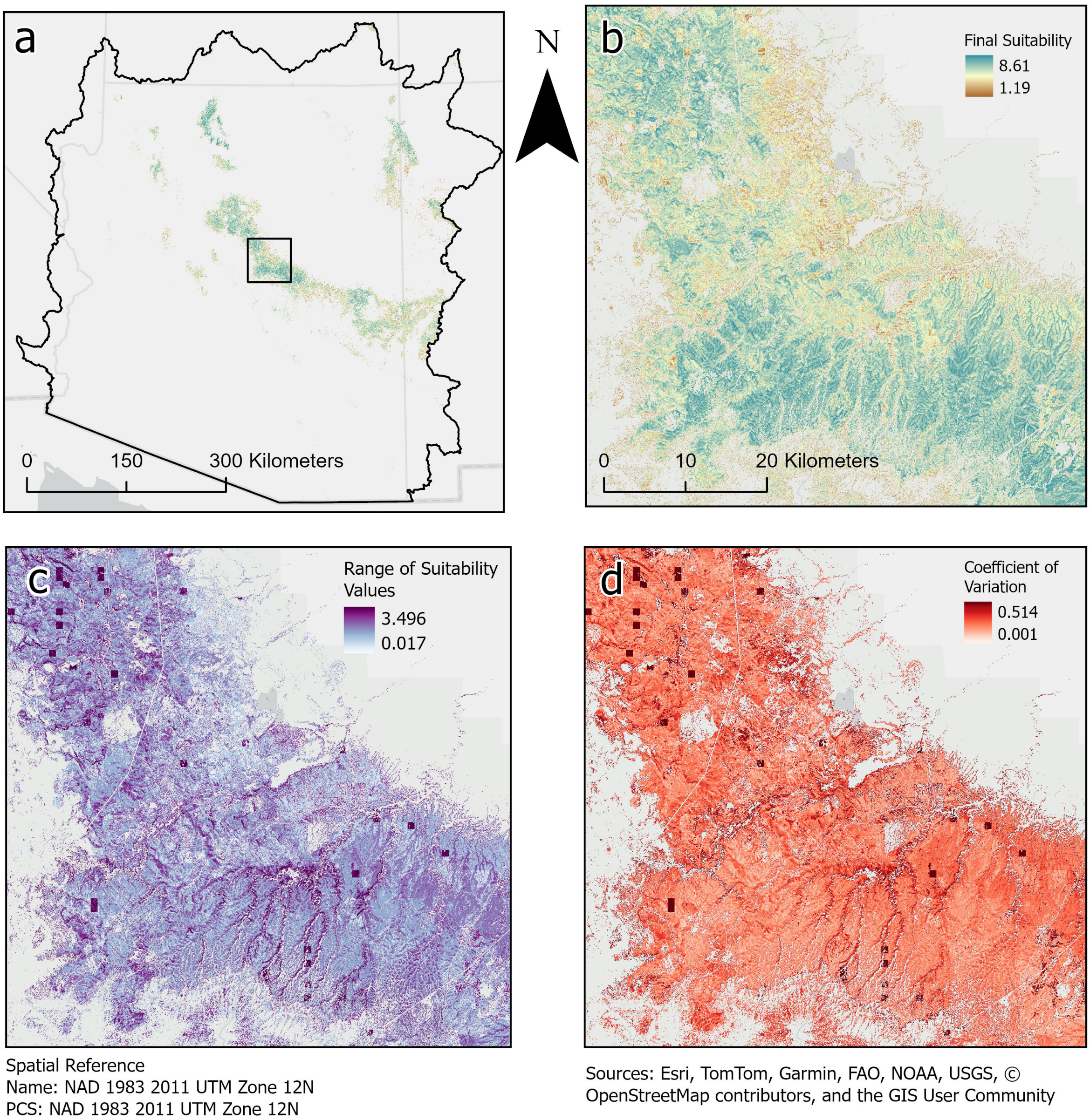

Figure 8: Suitability analysis area and variability in final suitability from sensitivity analysis. The chosen weighting for the final layer was [0.2,0.4,0.2,0.2]; in the sensitivity analysis, these weights were shuffled, resulting in four rasters for final suitability; in each one, a different variable was weighted with 0.4 while the rest were weighted 0.2. These rasters were stacked and pixel-wise coefficient of variation (CoV) and ranges were calculated. (a) shows the entire AZH8 Study area. (b) shows the zoomed-in area where the sensitivity analysis was conducted. (c) Shows the pixel-wise range in suitability values across all four weighting scenarios, and (d) shows the CoV across all four scenarios. The highest range (3.496) and highest CoV values (0.514) both occur in large square areas similar to the size of the 800m SF pixels before resampling, suggesting that sSF is responsible for the large shifts in suitability in those locations. These could represent noise in the precipitation dataset. Variability in pixel values is also rather high along stream networks, which mimics the variability in the SMII variable caused by a high weighting of sTRMI.

to start over and develop ways to include groundwater resources within their planning[105, 106, 107]. In 2024, the President's Council of Advisers on Science and Technology, as part of the Bipartisan Infrastructure Law and Inflation Reduction Act explicitly recommended acceleration in the development of collaborative databases and tools to address groundwater storage, withdraw and recharge at spatial scales useful to water managers and users[108]. This analysis offers an a new tool to assess potential groundwater recharge at landscape scales through forest management, allowing for groundwater recharge to be managed as a co-benefit of thinning for forest health and wildfire risk reduction.

One of the main challenges in mapping suitability at landscape scales is the lack of high-resolution data. Arizona lacks detailed hydrogeologic mapping throughout much of the state. The State Geologic map within the State Geologic Mapping Compilation contains geologic units and faults mapped to the 1:500,000 scale. However, digitized lineaments, particularly faults, are limited to very large faults state-wide and are almost completely absent in the northeastern part of the state on the Navajo Nation and Colorado Plateau.

Groundwater is and always has been difficult to monitor and measure. However, springs are convenient locations to monitor the effects of land management on groundwater recharge. Though tracer studies are needed to connect specific springs to particular recharge areas, continuous monitoring of springs and the base flow component of perennial spring-fed rivers can inform land managers of the effectiveness of thinning in enhancing recharge and help validate suitability analyses.

5. Acknowledgments

Thank you to the Arizona Board of Regents for funding this research through the Technology and Research Initiative Fund (TRIF) through the Arizona Tri-University Recharge and Water Reliability Project (ATUR). Thank you to all the members of ATUR for your support, guidance, and suggestions. Special thanks to Abdul Moiz for generating hydroclimate datasets used in this analysis.

6. Open research

The data, methods, and code base for this research can be found on github: https://github.com/Ryan3Lima/ATUR-Thinning-to-enhance-recharge , in the Open Sciences Framework Project associated with this work. The data will also be available on hydro-share.

7. Declaration of generative AI and AI-assisted technologies in the writing process

During the preparation of this work, the authors used ChatGPT4o and Research Rabbit to assist in our literature review. ChatGPT4o and Github Copilot were used in developing the Python code for the analysis tools created to combine and weight layers and conduct the sensitivity analyses. The authors reviewed and edited the content as needed and take full responsibility for the content of the published article.

References

[1] K. E. Bennett, C. Talsma, R. Boero, Concurrent Changes in Extreme Hydroclimate Events in the Colorado River Basin, Water 13 (7) (2021) 978. doi:10.3390/w13070978.
URL https://www.mdpi.com/2073-4441/13/7/978

[2] D. M. Meko, C. A. Woodhouse, A. G. Winitsky, Tree-Ring Perspectives on the Colorado River: Looking Back and Moving Forward, JAWRA Journal of the American Water Resources Association 58 (5) (2022) 604–621. doi:10.1111/1752-1688.12989.
URL https://onlinelibrary.wiley.com/doi/10.1111/1752-1688.12989

[3] A. P. Williams, B. I. Cook, J. E. Smerdon, Rapid intensification of the emerging southwestern North American megadrought in 2020–2021, Nature Climate Change 12 (3) (2022) 232–234. doi:10.1038/s41558-022-01290-z.
URL https://www.nature.com/articles/s41558-022-01290-z

[4] D. Hogan, J. D. Lundquist, Recent Upper Colorado River Streamflow Declines Driven by Loss of Spring Precipitation, Geophysical Research Letters 51 (16) (2024) e2024GL109826. doi:10.1029/2024GL109826.
URL https://agupubs.onlinelibrary.wiley.com/doi/10.1029/2024GL109826

[5] B. Udall, J. Overpeck, The twenty-first century Colorado River hot drought and implications for the future, Water Resources Research 53 (3) (2017) 2404–2418. doi:10.1002/2016WR019638.
URL https://agupubs.onlinelibrary.wiley.com/doi/10.1002/2016WR019638
[6] D. E. Tadych, M. Ford, B. G. Colby, L. E. Condon, Historical patterns of well drilling and groundwater depth in Arizona considering groundwater regulation and surface water access, JAWRA Journal of the American Water Resources Association (2024) 1752–1688.13234doi:10.1111/1752-1688.13234.
URL https://onlinelibrary.wiley.com/doi/10.1111/1752-1688.13234
[7] S. L. Castle, B. F. Thomas, J. T. Reager, M. Rodell, S. C. Swenson, J. S. Famiglietti, Groundwater depletion during drought threatens future water security of the colorado river basin, Geophysical Research Letters 41 (16) (2014) 5904–5911. doi:10.1002/2014GL061055.
URL https://agupubs.onlinelibrary.wiley.com/doi/10.1002/2014GL061055
[8] V. Iglesias, J. K. Balch, W. R. Travis, U.s. fires became larger, more frequent, and more widespread in the 2000s, Science Advances 8 (11) (03 2022). doi:10.1126/sciadv.abc0020.
URL http://dx.doi.org/10.1126/sciadv.abc0020
[9] W. Covington, M. M. Moore, Southwestern ponderosa pine forest structure: changes since Euro-American settlement, Journal of forestry. 92 (1994) 39–47, place: Bethesda, MD : Publisher: Society of American Foresters,.
[10] P. Friederici, Ecological Restoration of Southwestern Ponderosa Pine Forests, no. v.2 in Science Practice Ecological Restoration, Island Press, Chicago, 2013.
[11] C. D. Allen, M. Savage, D. A. Falk, K. F. Suckling, T. W. Swetnam, T. Schulke, P. B. Stacey, P. Morgan, M. Hoffman, J. T. Klingel, Ecological restoration of southwestern ponderosa pine ecosystems: a broad perspective, Ecological Applications 12 (5) (2002) 1418–1433. doi:10.1890/1051-0761(2002)012[1418:EROSPP]2.0.CO;2.
URL http://doi.wiley.com/10.1890/1051-0761(2002)012[1418:EROSPP]2.0.CO;2
[12] A. M. Youberg, J. B. Loverich, M. J. Kellogg, J. E. Fuller, Before the fire: Assessing post-wildfire flooding and debris-flow hazards for pre-disaster mitigation (03 2019).
URL http://dx.doi.org/10.5194/nhess-2019-74
[13] L. T. Berner, B. E. Law, A. J. H. Meddens, J. A. Hicke, Tree mortality from fires, bark beetles, and timber harvest during a hot and dry decade in the western United States (2003–2012), Environmental Research Letters 12 (6) (2017) 065005. doi:10.1088/1748-9326/aa6f94.
URL https://iopscience.iop.org/article/10.1088/1748-9326/aa6f94
[14] T. N. Wasserman, S. E. Mueller, Climate influences on future fire severity: a synthesis of climate-fire interactions and impacts on fire regimes, high-severity fire, and forests in the western united states, Fire Ecology 19 (1) (07 2023). doi:10.1186/s42408-023-00200-8.
URL http://dx.doi.org/10.1186/s42408-023-00200-8
[15] A. D. Del Campo, K. Otsuki, Y. Serengil, J. A. Blanco, R. Yousefpour, X. Wei, A global synthesis on the effects of thinning on hydrological processes: Implications for forest management, Forest Ecology and Management 519 (2022) 120324. doi:10.1016/j.foreco.2022.120324.
URL https://linkinghub.elsevier.com/retrieve/pii/S0378112722003188
[16] T. Sankey, J. Donald, J. McVay, M. Ashley, F. O'Donnell, S. M. Lopez, A. Springer, Multi-scale analysis of snow dynamics at the southern margin of the north american continental snow distribution, Remote Sensing of Environment 169 (2015) 307–319. doi:10.1016/j.rse.2015.08.028.
URL https://linkinghub.elsevier.com/retrieve/pii/S0034425715301140
[17] A. Belmonte, T. Sankey, J. Biederman, J. Bradford, S. Goetz, T. Kolb, Uav-based estimate of snow cover dynamics: Optimizing semi-arid forest structure for snow persistence, Remote Sensing 13 (5) (2021) 1036. doi:10.3390/rs13051036.
URL https://www.mdpi.com/2072-4292/13/5/1036
[18] J. Donager, T. T. Sankey, A. J. Sánchez Meador, J. B. Sankey, A. Springer, Integrating airborne and mobile lidar data with uav photogrammetry for rapid assessment of changing forest snow depth and cover, Science of Remote Sensing 4 (2021) 100029. doi:10.1016/j.srs.2021.100029.
URL https://linkinghub.elsevier.com/retrieve/pii/S266601722100016X
[19] A. Belmonte, T. Ts. Sankey, J. Biederman, J. B. Bradford, T. Kolb, Soil moisture response to seasonal drought conditions and post-thinning forest structure, Ecohydrology 15 (5) (2022) e2406. doi:10.1002/eco.2406.
URL https://onlinelibrary.wiley.com/doi/10.1002/eco.2406
[20] T. Sankey, J. Tatum, Thinning increases forest resiliency during unprecedented drought, Scientific Reports 12 (1) (2022) 9041. doi:10.1038/s41598-022-12982-z.
URL https://www.nature.com/articles/s41598-022-12982-z
[21] T. Sankey, A. Belmonte, R. Massey, J. Leonard, Regional-scale forest restoration effects on ecosystem resiliency to drought: a synthesis of vegetation and moisture trends on Google Earth Engine, Remote Sensing in Ecology and Conservation 7 (2) (2021) 259–274. doi:10.1002/rse2.186.
URL https://zslpublications.onlinelibrary.wiley.com/doi/10.1002/rse2.186
[22] J. Bosch, J. Hewlett, A review of catchment experiments to determine the effect of vegetation changes on water yield and evapotranspiration, Journal of Hydrology 55 (1-4) (1982) 3–23. doi:10.1016/0022-1694(82)90117-2.
URL https://linkinghub.elsevier.com/retrieve/pii/0022169482901172
[23] M. B. Baker, Effects of Ponderosa Pine Treatments on Water Yield in Arizona, Water Resources Research 22 (1) (1986) 67–73. doi:10.1029/WR022i001p00067.
URL https://agupubs.onlinelibrary.wiley.com/doi/10.1029/WR022i001p00067
[24] G. J. Gottfried, Moderate timber harvesting increases water yields from an Arizona Mixed Conifer Watershed, JAWRA

Journal of the American Water Resources Association 27 (3) (1991) 537–546, publisher: John Wiley & Sons, Ltd.
URL https://onlinelibrary.wiley.com/doi/abs/10.1111/j.1752-1688.1991.tb01454.x
[25] B. D. Smerdon, T. Redding, J. Beckers, An overview of the effects of forest management on groundwater hydrology, Journal of Ecosystems and Management (Mar. 2009). doi:10.22230/jem.2009v10n1a409.
URL https://jem-online.org/index.php/jem/article/view/409
[26] C. B. Zou, P. F. Ffolliott, M. Wine, Streamflow responses to vegetation manipulations along a gradient of precipitation in the Colorado River Basin, Forest Ecology and Management 259 (7) (2010) 1268–1276. doi:10.1016/j.foreco.2009.08.005.
URL https://linkinghub.elsevier.com/retrieve/pii/S0378112709005350
[27] C. J. W. Wyatt, Estimating groundwater yield following forest restoration along the mogollon rim, Ph.D. thesis, Flagstaff, AZ (2013).
URL https://cdm17192.contentdm.oclc.org/digital/collection/p17192coll1/id/476/rec/3
[28] H. A. Moreno, H. V. Gupta, D. D. White, D. A. Sampson, Modeling the distributed effects of forest thinning on the long-term water balance and stream flow extremes for a semi-arid basin in the southwestern US (Oct. 2015). doi:10.5194/hessd-12-10827-2015.
URL https://hess.copernicus.org/preprints/12/10827/2015/hessd-12-10827-2015.pdf
[29] S. Simonit, J. P. Connors, J. Yoo, A. Kinzig, C. Perrings, The Impact of Forest Thinning on the Reliability of Water Supply in Central Arizona, PLOS ONE 10 (4) (2015) e0121596. doi:10.1371/journal.pone.0121596.
URL https://dx.plos.org/10.1371/journal.pone.0121596
[30] C. Wyatt, F. C. O'Donnell, A. E. Springer, Semi-arid aquifer responses to forest restoration treatments and climate change, Ground Water (2015). doi:10.1111/gwat.12184.
[31] F. C. O'Donnell, W. T. Flatley, A. E. Springer, P. Z. Fulé, Forest restoration as a strategy to mitigate climate impacts on wildfire, vegetation, and water in semiarid forests, Ecological Applications 28 (6) (2018) 1459–1472. doi:10.1002/eap.1746.
URL https://esajournals.onlinelibrary.wiley.com/doi/10.1002/eap.1746
[32] A. R. Hibbert, Managing vegetation to increase flow in the colorado river basin, Tech. rep., Fort Collins, CO (1979).
[33] J. A. Biederman, M. D. Robles, R. L. Scott, J. F. Knowles, Streamflow response to wildfire differs with season and elevation in adjacent headwaters of the lower colorado river basin, Water Resources Research 58 (3) (2022) e2021WR030687. doi:10.1029/2021WR030687.
URL https://agupubs.onlinelibrary.wiley.com/doi/10.1029/2021WR030687
[34] R. Moore, S. Wondzell, Physical hydrology and the effects of forest harvesting in the pacific northwest: A review, Journal of the American Water Resources Association 41 (4) (2005) 763–784. doi:10.1111/j.1752-1688.2005.tb04463.x.
URL http://doi.wiley.com/10.1111/j.1752-1688.2005.tb04463.x
[35] J. A. Stanturf, B. J. Palik, R. K. Dumroese, Contemporary forest restoration: A review emphasizing function, Forest Ecology and Management 331 (2014) 292–323. doi:10.1016/j.foreco.2014.07.029.
URL https://linkinghub.elsevier.com/retrieve/pii/S0378112714004654
[36] S. Filoso, M. Bezerra, K. C. B. Weiss, M. A. Palmer, Impacts of forest restoration on water yield: A systematic review, PLOS ONE 12 (8) (2017) e0183210. doi:10.1371/journal.pone.0183210.
URL https://dx.plos.org/10.1371/journal.pone.0183210
[37] F. C. O'Donnell, The influence of restoration treatments on hydrologic output in fire-adapted forests of the southwest, Tech. rep., Flagstaff, AZ (11 2016).
URL https://cdm17192.contentdm.oclc.org/digital/collection/p17192coll1/id/662/rec/1
[38] J. M. Mueller, A. B. Soder, A. E. Springer, Valuing attributes of forest restoration in a semi-arid watershed, Landscape and Urban Planning 184 (2019) 78–87. doi:10.1016/j.landurbplan.2018.12.012.
URL https://linkinghub.elsevier.com/retrieve/pii/S0169204618304535
[39] A. B. Soder, J. M. Mueller, A. E. Springer, K. E. LaPine, Geospatial analysis of nonmarket values to prioritize forest restoration, Land 11 (9) (2022) 1387. doi:10.3390/land11091387.
URL https://www.mdpi.com/2073-445X/11/9/1387
[40] M. E. Campana, Groundwater management: Quo vadis?, Water Resources IMPACT 16 (1) (2014). doi:10.2307/wateresoimpa.16.1.0026.
URL www.jstor.org/stable/pdf/wateresoimpa.16.1.0026.pdf
[41] S. B. Megdal, A. K. Gerlak, R. G. Varady, L. Huang, Groundwater governance in the united states: Common priorities and challenges, Groundwater 53 (5) (2014) 677–684. doi:10.1111/gwat.12294.
URL http://dx.doi.org/10.1111/gwat.12294
[42] T. C. Brown, M. T. Hobbins, J. A. Ramirez, The Source of Water Supply in the United States, Discussion Paper RMRS-RWU-4851, U.S. Department of Agriculture, Forest Service, Rocky Mountain Research Station, Fort Collins, CO (2005).
URL https://www.researchgate.net/profile/Jorge-Ramirez-14/publication/266272409_The_source_of_water_supply_in_the_United_States/links/54b5fcb50cf26833efd34687/The-source-of-water-supply-in-the-United-States.pdf
[43] K. Hansen, B. Gaolach, S. Buck, R. Heinse, D. Godwin, G. Paige, H. Braithwaite, T. Warziniack, S. Fernald, The western water network: A vision for the future of water management in the west, Tech. rep. (01 2024).
[44] B. Blagojević, R. Jonsson, R. Björheden, E.-M. Nordström, O. Lindroos, Multi-criteria decision analysis (mcda) in forest operations – an introductional review, Croat. j. for. eng. (2019).
[45] G. Mendoza, H. Martins, Multi-criteria decision analysis in natural resource management: A critical review of methods and new modelling paradigms, Forest Ecology and Management 230 (1-3) (2006) 1–22. doi:10.1016/j.foreco.2006.03.023.

URL https://linkinghub.elsevier.com/retrieve/pii/S0378112706002258
[46] J. Malczewski, Gis-based multicriteria decision analysis: a survey of the literature, International Journal of Geographical Information Science 20 (7) (2006) 703–726. doi:10.1080/13658810600661508.
URL http://www.tandfonline.com/doi/abs/10.1080/13658810600661508
[47] S. Fathi, J. Hagen, A. Matanó, G. E. H. Nogueira, Review of GIS Multi-Criteria Decision Analysis for Managed Aquifer Recharge in Semi-Arid Regions, Springer International Publishing, Cham, 2021, pp. 19–52, dOI: 10.1007/978-3-030-68124-1_2. doi:10.1007/978-3-030-68124-1_2.
URL https://link.springer.com/10.1007/978-3-030-68124-1_2
[48] P. Raja Shekar, A. Mathew, Assessing groundwater potential zones and artificial recharge sites in the monsoon-fed murredu river basin, india: An integrated approach using gis, ahp, and fuzzy-ahp, Groundwater for Sustainable Development 23 (2023) 100994. doi:10.1016/j.gsd.2023.100994.
URL https://linkinghub.elsevier.com/retrieve/pii/S2352801X23000942
[49] M. A. Rahman, B. Rusteberg, R. Gogu, J. Lobo Ferreira, M. Sauter, A new spatial multi-criteria decision support tool for site selection for implementation of managed aquifer recharge, Journal of Environmental Management 99 (2012) 61–75. doi:10.1016/j.jenvman.2012.01.003.
URL http://dx.doi.org/10.1016/j.jenvman.2012.01.003
[50] A. Shaban, M. Khawlie, C. Abdallah, Use of remote sensing and gis to determine recharge potential zones: the case of occidental lebanon, Hydrogeology Journal 14 (4) (2006) 433–443. doi:10.1007/s10040-005-0437-6.
URL http://link.springer.com/10.1007/s10040-005-0437-6
[51] J. T. Parker, W. C. Steinkampf, M. E. Flynn, Hydrogeology of the mogollon highlands, central arizona, Tech. rep., Reston, VA, series: Scientific Investigations Report (2005).
URL https://pubs.usgs.gov/sir/2004/5294/pdf/Parker%20SIR%202004-5294%20WEB.pdf
[52] B. W. Tobin, A. E. Springer, D. K. Kreamer, E. Schenk, Review: The distribution, flow, and quality of grand canyon springs, arizona (usa), Hydrogeology Journal 26 (3) (2018) 721–732. doi:10.1007/s10040-017-1688-8.
URL http://link.springer.com/10.1007/s10040-017-1688-8
[53] C. J. R. Jones, A. E. Springer, B. W. Tobin, S. J. Zappitello, N. A. Jones, Characterization and hydraulic behaviour of the complex karst of the kaibab plateau and grand canyon national park, usa, Geological Society, London, Special Publications 466 (1) (2018) 237–260. doi:10.1144/SP466.5.
URL https://www.lyellcollection.org/doi/10.1144/SP466.5
[54] P. W. Huntoon, The karstic groundwater basins of the kaibab plateau, arizona, Water Resources Research 10 (3) (1974) 579–590. doi:10.1029/WR010i003p00579.
URL https://agupubs.onlinelibrary.wiley.com/doi/10.1029/WR010i003p00579
[55] M. B. Baker, Chapter 10: Hydrology, no. v.2 in Science Practice Ecological Restoration, Island Press, Chicago, 2013, pp. 161–174.
[56] C. Eastoe, Isotope record of groundwater recharge mechanisms and climate change in southwestern north america, Applied Geochemistry 151 (2023) 105604. doi:10.1016/j.apgeochem.2023.105604.
URL https://linkinghub.elsevier.com/retrieve/pii/S0883292723000495
[57] S. Earman, A. R. Campbell, F. M. Phillips, B. D. Newman, Isotopic exchange between snow and atmospheric water vapor: Estimation of the snowmelt component of groundwater recharge in the southwestern united states, Journal of Geophysical Research: Atmospheres 111 (D9) (2006) 2005JD006470. doi:10.1029/2005JD006470.
URL https://agupubs.onlinelibrary.wiley.com/doi/10.1029/2005JD006470
[58] C. J. W. Wyatt, Estimating groundwater yield following forest restoration along the Mogollon Rim, Master's thesis, Northern Arizona University, Flagstaff, AZ (2013).
URL https://cdm17192.contentdm.oclc.org/digital/collection/p17192coll1/id/476/rec/3
[59] C. A. Schultz, T. Jedd, R. D. Beam, The Collaborative Forest Landscape Restoration Program: A History and Overview of the First Projects, Journal of Forestry 110 (7) (2012) 381–391. doi:10.5849/jof.11-082.
URL https://academic.oup.com/jof/article/110/7/381-391/4599006
[60] F. C. O'Donnell, J. Donager, T. Sankey, S. Masek Lopez, A. E. Springer, Vegetation structure controls on snow and soil moisture in restored ponderosa pine forests, Hydrological Processes 35 (11) (2021) e14432. doi:10.1002/hyp.14432.
URL https://onlinelibrary.wiley.com/doi/10.1002/hyp.14432
[61] K. M. Donovan, A. E. Springer, B. W. Tobin, R. A. Parnell, Karst Spring Processes and Storage Implications in High Elevation, Semiarid Southwestern United States, 1st Edition, Wiley, 2022, pp. 35–50, dOI: 10.1002/9781119818625.ch4. doi:10.1002/9781119818625.ch4.
URL https://agupubs.onlinelibrary.wiley.com/doi/10.1002/9781119818625.ch4
[62] K. W. Blasch, J. P. Hoffmann, L. F. Graser, J. R. Bryson, A. L. Flint, Hydrogeology of the upper and middle verde river watersheds, central arizona, Tech. rep., series: Scientific Investigations Report (2006).
URL https://pubs.usgs.gov/sir/2005/5198/pdf/sir20055198.pdf
[63] A. E. Springer, E. M. Boldt, K. M. Junghans, Local vs. regional groundwater flow delineation from stable isotopes at western north america springs, Groundwater 55 (1) (2017) 100–109. doi:10.1111/gwat.12442.
URL https://ngwa.onlinelibrary.wiley.com/doi/10.1111/gwat.12442
[64] L. P. Kerhoulas, T. E. Kolb, G. W. Koch, Tree size, stand density, and the source of water used across seasons by ponderosa pine in northern arizona, Forest Ecology and Management 289 (2013) 425–433. doi:10.1016/j.foreco.2012.10.036.
URL https://linkinghub.elsevier.com/retrieve/pii/S0378112712006330
[65] L. P. Kerhoulas, N. Umstattd, G. W. Koch, Seasonal water source patterns in a northern arizona pine forest, Frontiers in Forests and Global Change 6 (2023) 1150413. doi:10.3389/ffgc.2023.1150413.

URL https://www.frontiersin.org/articles/10.3389/ffgc.2023.1150413/full
[66] R. Dwivedi, J. A. Biederman, P. D. Broxton, J. K. Pearl, K. Lee, B. M. Svoma, W. J. D. Van Leeuwen, M. D. Robles, How three-dimensional forest structure regulates the amount and timing of snowmelt across a climatic gradient of snow persistence, Frontiers in Water 6 (2024) 1374961. doi:10.3389/frwa.2024.1374961.
URL https://www.frontiersin.org/articles/10.3389/frwa.2024.1374961/full
[67] J. A. Biederman, A. J. Somor, A. A. Harpold, E. D. Gutmann, D. D. Breshears, P. A. Troch, D. J. Gochis, R. L. Scott, A. J. H. Meddens, P. D. Brooks, Recent tree die-off has little effect on streamflow in contrast to expected increases from historical studies, Water Resources Research 51 (12) (2015) 9775–9789. doi:10.1002/2015WR017401.
URL https://agupubs.onlinelibrary.wiley.com/doi/10.1002/2015WR017401
[68] H. D. Adams, C. H. Luce, D. D. Breshears, C. D. Allen, M. Weiler, V. C. Hale, A. M. S. Smith, T. E. Huxman, Ecohydrological consequences of drought- and infestation- triggered tree die-off: insights and hypotheses, Ecohydrology 5 (2) (2012) 145–159. doi:10.1002/eco.233.
URL https://onlinelibrary.wiley.com/doi/10.1002/eco.233
[69] R. W. Carroll, J. L. Huntington, K. A. Snyder, R. G. Niswonger, C. Morton, T. K. Stringham, Evaluating mountain meadow groundwater response to Pinyon-Juniper and temperature in a great basin watershed, Ecohydrology 10 (1) (2016) e1792. doi:10.1002/eco.1792.
URL https://onlinelibrary.wiley.com/doi/10.1002/eco.1792
[70] J. M. Frank, W. J. Massman, B. E. Ewers, D. G. Williams, Bayesian analyses of 17 winters of water vapor fluxes show bark beetles reduce sublimation, Water Resources Research 55 (2) (2019) 1598–1623. doi:10.1029/2018wr023054.
URL http://dx.doi.org/10.1029/2018WR023054
[71] J. F. Knowles, N. R. Bjarke, A. M. Badger, M. Berkelhammer, J. A. Biederman, P. D. Blanken, M. Bretfeld, S. P. Burns, B. E. Ewers, J. M. Frank, J. A. Hicke, L. Lestak, B. Livneh, D. E. Reed, R. L. Scott, N. P. Molotch, Bark beetle impacts on forest evapotranspiration and its partitioning, Science of The Total Environment 880 (2023) 163260. doi:10.1016/j.scitotenv.2023.163260.
URL http://dx.doi.org/10.1016/j.scitotenv.2023.163260
[72] A. A. Harpold, J. A. Biederman, K. Condon, M. Merino, Y. Korgaonkar, T. Nan, L. L. Sloat, M. Ross, P. D. Brooks, Changes in snow accumulation and ablation following the las conchas forest fire, new mexico, usa, Ecohydrology 7 (2) (2013) 440–452. doi:10.1002/eco.1363.
URL http://dx.doi.org/10.1002/eco.1363
[73] R. Dwivedi, J. A. Biederman, P. D. Broxton, J. K. Pearl, K. Lee, B. M. Svoma, W. J. D. Van Leeuwen, M. D. Robles, How three-dimensional forest structure regulates the amount and timing of snowmelt across a climatic gradient of snow persistence, Frontiers in Water 6 (2024) 1374961. doi:10.3389/frwa.2024.1374961.
URL https://www.frontiersin.org/articles/10.3389/frwa.2024.1374961/full
[74] J. A. Biederman, A. A. Harpold, D. J. Gochis, B. E. Ewers, D. E. Reed, S. A. Papuga, P. D. Brooks, Increased evaporation following widespread tree mortality limits streamflow response, Water Resources Research 50 (7) (2014) 5395–5409. doi:10.1002/2013wr014994.
URL http://dx.doi.org/10.1002/2013WR014994
[75] W. Veatch, P. D. Brooks, J. R. Gustafson, N. P. Molotch, 'quantifying the effects of forest canopy cover on net snow accumulation at a continental, mid-latitude site', Ecohydrology 2 (2) (2009) 115–128. doi:10.1002/eco.45.
URL http://dx.doi.org/10.1002/eco.45
[76] P. D. Broxton, W. J. van Leeuwen, J. A. Biederman, Forest cover and topography regulate the thin, ephemeral snowpacks of the semiarid southwest united states, Ecohydrology 13 (4) (02 2020). doi:10.1002/eco.2202.
URL http://dx.doi.org/10.1002/eco.2202
[77] A. D. Del Campo, M. González-Sanchis, A. J. Molina, A. García-Prats, C. J. Ceacero, I. Bautista, Effectiveness of water-oriented thinning in two semiarid forests: The redistribution of increased net rainfall into soil water, drainage and runoff, Forest Ecology and Management 438 (2019) 163–175. doi:10.1016/j.foreco.2019.02.020.
URL https://linkinghub.elsevier.com/retrieve/pii/S0378112718323533
[78] A. J. Parker, The topographic relative moisture index: An approach to soil-moisture assessment in mountain terrain, Physical Geography 3 (2) (1982) 160–168. doi:10.1080/02723646.1982.10642224.
URL https://www.tandfonline.com/doi/full/10.1080/02723646.1982.10642224
[79] J. Jasiewicz, T. F. Stepinski, Geomorphons — a pattern recognition approach to classification and mapping of landforms, Geomorphology 182 (2013) 147–156. doi:10.1016/j.geomorph.2012.11.005.
URL https://linkinghub.elsevier.com/retrieve/pii/S0169555X12005028
[80] W. Woessner, E. Poeter, Hydrogeologic properties of earth materials and principles of groundwater flow (2020). doi:10.21083/978-1-7770541-2-0.
URL http://dx.doi.org/10.21083/978-1-7770541-2-0
[81] J. Huscroft, T. Gleeson, J. Hartmann, J. Börker, Compiling and mapping global permeability of the unconsolidated and consolidated earth: Global hydrogeology maps 2.0 (glhymps 2.0), Geophysical Research Letters 45 (4) (2018) 1897–1904. doi:10.1002/2017GL075860.
URL https://agupubs.onlinelibrary.wiley.com/doi/10.1002/2017GL075860
[82] R. A. Freeze, J. A. Cherry, Groundwater, Prentice-Hall, Englewood Cliffs, N.J, 1979.
[83] D. O'leary, J. Friedman, H. Pohn, Lineament, linear, lineation: Some proposed new standards for old terms, Geological Society of America Bulletin 87 (10) (1976).
[84] P. Sander, Lineaments in groundwater exploration: a review of applications and limitations, Hydrogeology Journal 15 (1) (2007) 71–74. doi:10.1007/s10040-006-0138-9.

URL http://link.springer.com/10.1007/s10040-006-0138-9
[85] A. Meijerink, D. Bannert, O. Batelaan, Remote sensing applications to groundwater, UNESCO, Paris, France, 2007.
[86] M. Nyborg, J. Berglund, C.-A. Triumf, Detection of lineaments using airborne laser scanning technology: Laxemar-simpevarp, sweden, Hydrogeology Journal 15 (1) (2007) 29–32. doi:10.1007/s10040-006-0134-0.
URL http://link.springer.com/10.1007/s10040-006-0134-0
[87] D. Ford, P. Williams, Karst Hydrogeology and Geomorphology, John Wiley and Sons, Ltd, 2007.
URL https://onlinelibrary.wiley.com/doi/book/10.1002/9781118684986
[88] N. Krešić, Water in karst: management, vulnerability, and restoration, McGraw-Hill, New York, NY, 2013.
[89] T. Halihan, C. M. Wicks, Modeling of storm responses in conduit flow aquifers with reservoirs, Journal of Hydrology 208 (1-2) (1998) 82–91. doi:10.1016/s0022-1694(98)00149-8.
URL http://dx.doi.org/10.1016/S0022-1694(98)00149-8
[90] X. Zeng, P. Broxton, N. Dawson, Snowpack change from 1982 to 2016 over conterminous united states, Geophysical Research Letters 45 (23) (12 2018). doi:10.1029/2018gl079621.
URL http://dx.doi.org/10.1029/2018GL079621
[91] C. Daly, M. Halbleib, J. I. Smith, W. P. Gibson, M. K. Doggett, G. H. Taylor, J. Curtis, P. P. Pasteris, Physiographically sensitive mapping of climatological temperature and precipitation across the conterminous united states, International Journal of Climatology 28 (15) (2008) 2031–2064. doi:10.1002/joc.1688.
URL http://dx.doi.org/10.1002/joc.1688
[92] P. D. Broxton, X. Zeng, N. Dawson, Why do global reanalyses and land data assimilation products underestimate snow water equivalent?, Journal of Hydrometeorology 17 (11) (2016) 2743–2761. doi:10.1175/jhm-d-16-0056.1.
URL http://dx.doi.org/10.1175/JHM-D-16-0056.1
[93] P. Broxton, M. R. Ehsani, A. Behrangi, Improving mountain snowpack estimation using machine learning with sentinel-1, the airborne snow observatory, and university of arizona snowpack data, Earth and Space Science 11 (3) (03 2024). doi:10.1029/2023ea002964.
URL http://dx.doi.org/10.1029/2023EA002964
[94] P. C. Saksa, M. H. Conklin, J. J. Battles, C. L. Tague, R. C. Bales, Forest thinning impacts on the water balance of sierra nevada mixed-conifer headwater basins, Water Resources Research 53 (7) (2017) 5364–5381. doi:10.1002/2016wr019240.
URL http://dx.doi.org/10.1002/2016WR019240
[95] M. A. Battaglia, W. D. Shepperd, Chapter 2: Ponderosa Pine, Mixed Conifer, and Spruce-fir Forests, USDA Forest Service, Rocky Mountain Research Station, Fort Collins, CO, 2007.
URL https://www.researchgate.net/profile/Mike-Battaglia/publication/259601557_Ponderosa_pine_mixed_conifer_and_spruce-fir_forests/links/0deec52d8aabe8362e000000/Ponderosa-pine-mixed-conifer-and-spruce-fir-forests.pdf?_tp=eyJjb250ZXh0Ijp7ImZpcnN0UGFnZSI6InB1YmxpY2F0aW9uIiwicGFnZSI6InB1YmxpY2F0aW9uIn19
[96] K. L. Riley, I. C. Grenfell, J. D. Shaw, M. A. Finney, Treemap 2016 dataset generates conus-wide maps of forest characteristics including live basal area, aboveground carbon, and number of trees per acre, Journal of Forestry 120 (6) (2022) 607–632. doi:10.1093/jofore/fvac022.
URL https://academic.oup.com/jof/article/120/6/607/6701541
[97] J. De Reu, J. Bourgeois, M. Bats, A. Zwertvaegher, V. Gelorini, P. De Smedt, W. Chu, M. Antrop, P. De Maeyer, P. Finke, M. Van Meirvenne, J. Verniers, P. Crombé, Application of the topographic position index to heterogeneous landscapes, Geomorphology 186 (2013) 39–49. doi:10.1016/j.geomorph.2012.12.015.
URL http://dx.doi.org/10.1016/j.geomorph.2012.12.015
[98] I. Chenini, A. B. Mammou, M. El May, Groundwater recharge zone mapping using gis-based multi-criteria analysis: A case study in central tunisia (maknassy basin), Water Resources Management 24 (5) (2010) 921–939. doi:10.1007/s11269-009-9479-1.
URL http://link.springer.com/10.1007/s11269-009-9479-1
[99] A. Chowdhury, M. K. Jha, V. M. Chowdary, Delineation of groundwater recharge zones and identification of artificial recharge sites in west medinipur district, west bengal, using rs, gis and mcdm techniques, Environmental Earth Sciences 59 (6) (2010) 1209–1222. doi:10.1007/s12665-009-0110-9.
URL http://link.springer.com/10.1007/s12665-009-0110-9
[100] R. Al-Adamat, The use of gis and google earth for preliminary site selection of groundwater recharge in the azraq oasis area—jordan, Journal of Water Resource and Protection 04 (06) (2012) 395–399. doi:10.4236/jwarp.2012.46045.
URL http://www.scirp.org/journal/doi.aspx?DOI=10.4236/jwarp.2012.46045
[101] D. J. Weary, D. H. Doctor, Karst in the united states: A digital map compilation and database, Tech. rep., Reston, VA, series: Open-File Report (2014).
URL https://pubs.usgs.gov/of/2014/1156/pdf/of2014-1156.pdf
[102] E. Stewart, M. Williams, Record of decision for the four forest restoration initiative, Tech. rep. (04 2025).
URL https://www.fs.usda.gov/Internet/FSE_DOCUMENTS/stelprd3836454.pdf
[103] J. Credo, J. Torkelson, T. Rock, J. C. Ingram, Quantification of elemental contaminants in unregulated water across western navajo nation, International Journal of Environmental Research and Public Health 16 (15) (2019) 2727. doi:10.3390/ijerph16152727.
URL https://www.mdpi.com/1660-4601/16/15/2727
[104] L. Jones, J. C. Ingram, Invited perspective: Tribal water issues exemplified by the navajo nation, Environmental Health Perspectives 130 (12) (2022) 121301. doi:10.1289/EHP12187.
URL https://ehp.niehs.nih.gov/doi/10.1289/EHP12187
[105] U.S. House Committee on Agriculture, Hearing on the u.s. forest service's proposed groundwater directive, Tech. rep.,

accessed: 2025-02-17 (2014).
URL https://www.govinfo.gov/content/pkg/CHRG-113hhrg89799/html/CHRG-113hhrg89799.htm

[106] Lexology, U.s. forest service withdraws proposed groundwater directive, Tech. rep., accessed: 2025-02-17 (2014).
URL https://www.lexology.com/library/detail.aspx?g=c206481f-b49c-408b-b714-3fd798532ce6

[107] U.S. Forest Service, Proposed directive on groundwater resource management, Tech. rep., accessed: 2025-02-17 (2014).
URL https://www.federalregister.gov/documents/2014/05/06/2014-10366/proposed-directive-on-groundwater-resource-management-forest-service-manual-2560

[108] President's Council of Advisors on Science and Technology, F. Arnold, A. Prabhakar, M. Zuber, D. Arvizu, D. Assanis, J. Banovetz, L. Cooper, J. Dabiri, W. Dally, S. Desmond-Hellmann, I. Fung, A. Goldsmith, L. Greene, P. Hammond, E. Horvitz, J. Kiani, J. Levin, S. Pacala, S. Perlmutter, W. Press, J. Richeson, V. Sato, L. Su, K. Sullivan, T. Tao, P. Venables, C. Woteki, Pcast: Report to the president on improving groundwater security in the united states, Tech. rep., Executive Office of the President, dOI: 10.2172/2481670 (12 2024). doi:10.2172/2481670.
URL https://www.osti.gov/servlets/purl/2481670/

[109] C. L. Salui, Methodological validation for automated lineament extraction by line method in pci geomatica and matlab based hough transformation, Journal of the Geological Society of India 92 (3) (2018) 321–328. doi:10.1007/s12594-018-1015-6.
URL http://dx.doi.org/10.1007/s12594-018-1015-6

8. Appendix

8.1. Additional Figures

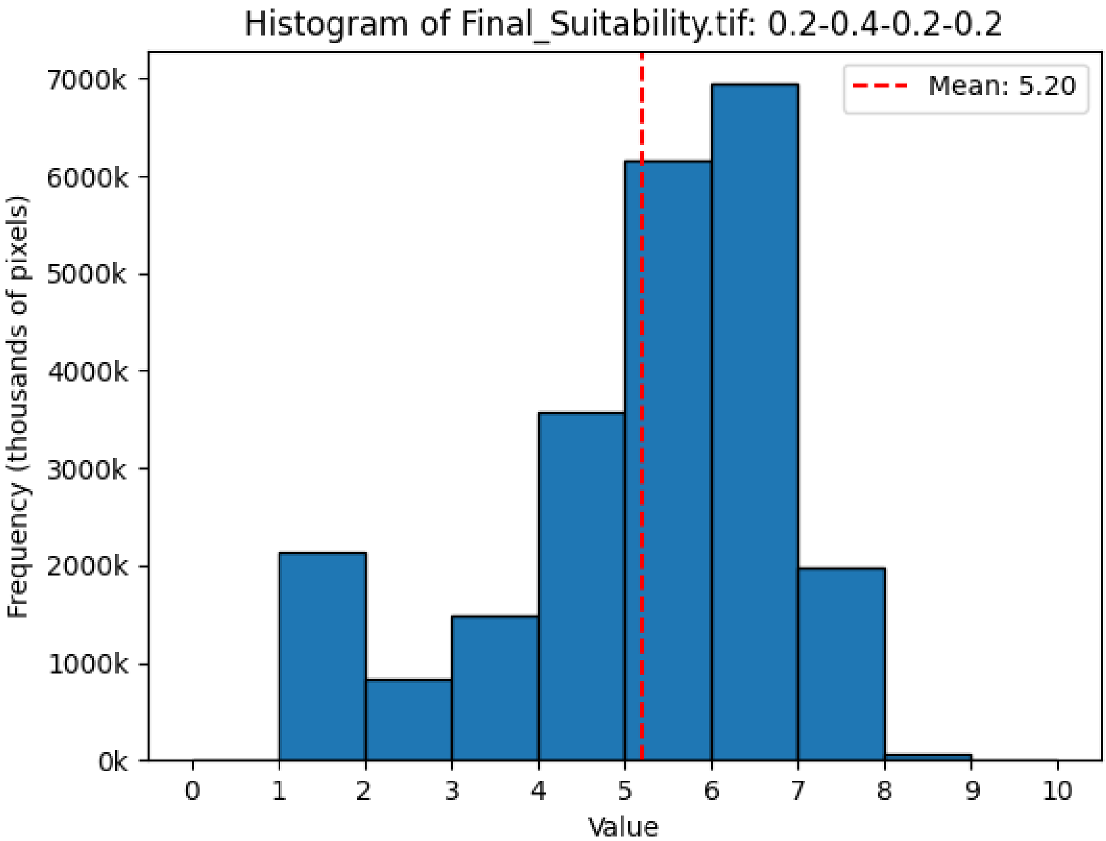

Figure 9: Histogram of pixel values of suitability for thinning to enhance recharge statewide.

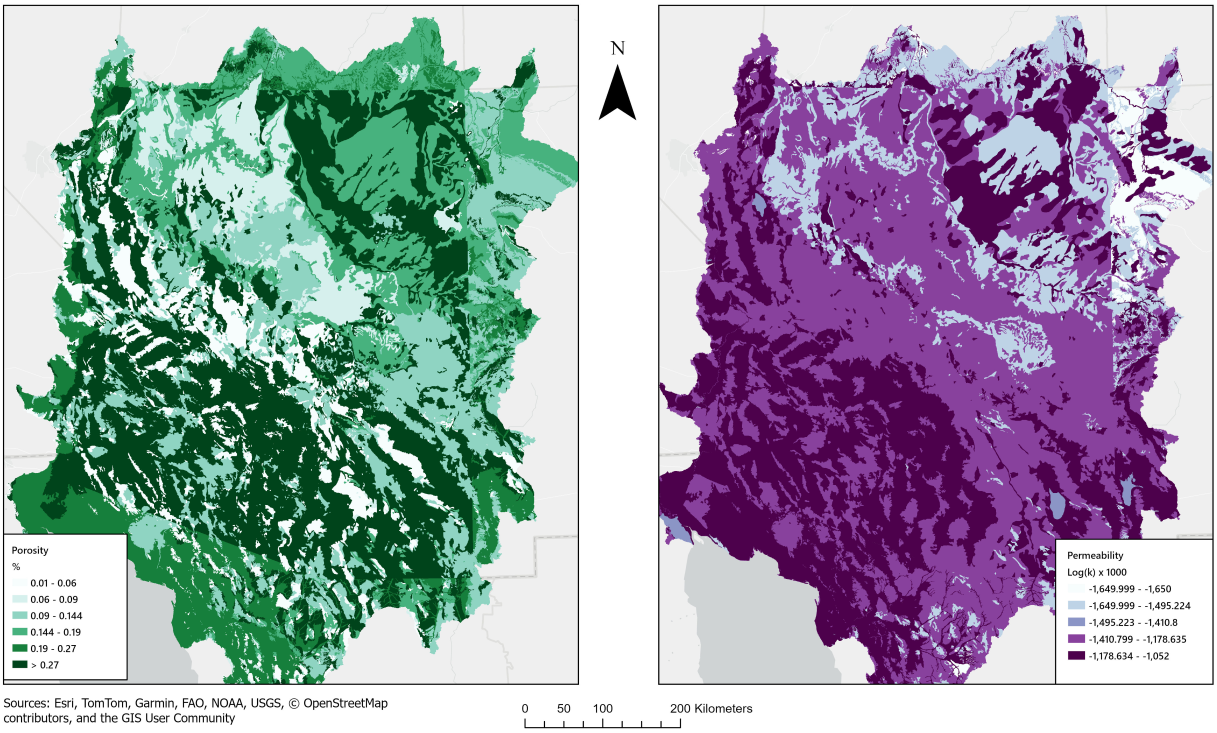

Figure 10: Matrix permeability and porosity values from GLHYMPS v2 rasterized and clipped to the AZH8 Study Area. Porosity values (Po) are shown in the left panel with darker green colors representing higher Po and lighter greens indicating lower Po. The panel on the right shows permeability (Pm) with areas of higher Pm in dark purple and lower Pm in lighter purples. These values represent the primary Pm and Po of the near-surface bedrock matrix but do not reflect secondary or tertiary Pm and Po caused by fractures, faults, or sinks. Note also that the scale of this geologic mapping does not represent stream channels, which may be areas of higher Pm. These values largely represent diffuse recharge potential.

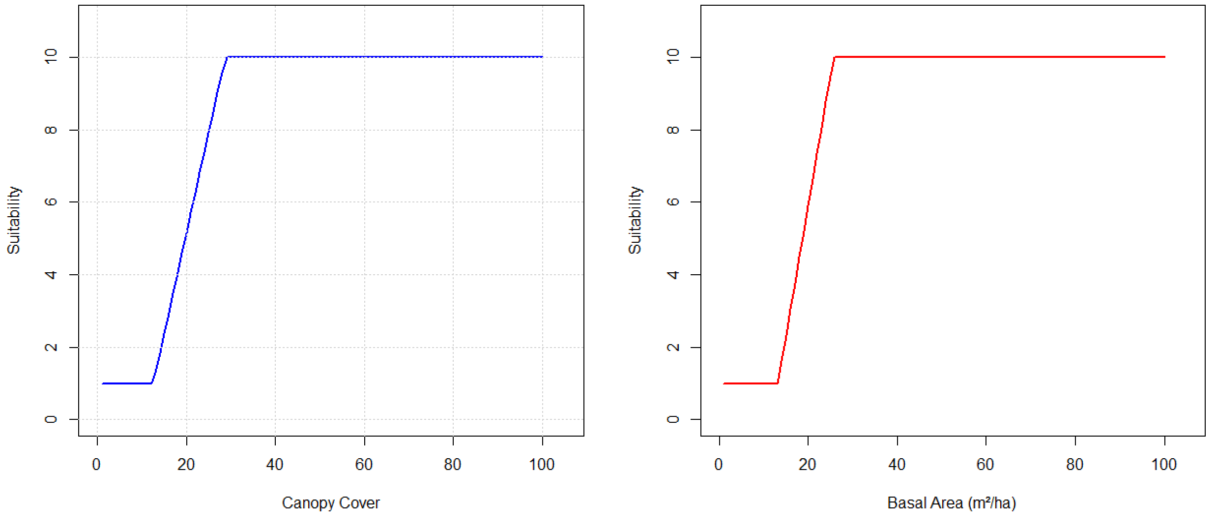

Figure 11: Canopy Cover and basal area rescaling functions for forest thinning suitability. Minimum and maximum threshold values for canopy cover are 12.5% and 28.75% respectively. Minimum and maximum threshold values for basal area are 13.15 (m^2 ha^-1) and 25.71 (m^2 ha^-1) respectively.

8.2. Addtional Methods

8.2.1. VDI

8.2.2. SMII

Table 2: Hydraulic Conductivity (Ksat) using a depth weighted average for 0 - 200 cm, Standard classes from Very Low to Very High, reclassified suitability values 1-10, and presence or absence within the study area.

Ksat	Standard Class	Assigned suitability score	Present in Study Area
0.0 - 0.01	Very Low	1	No
0.01 - 0.1	Low	2	No
0.1 - 1	Moderately Low	4	Yes
1 - 10	Moderately High	6	Yes
10 - 100	High	8	Yes
100 - 705	Very High	10	Yes

Table 3: Geomorphon landforms and associated suitability values depicting wetness values associated with those landforms from lowest (1) to highest (20).

Geomorphon landform	Wetness value (1-20)
Pit	20
Valley	18
Hollow	14

Geomorphon landform	Wetness value (1-20)
Footslope	12
Flat	10
Slope	8
Spur	6
Shoulder	4
Ridge	2
Peak	1

Table 4: Slope steepness and the wetness value (1-10) which is summed as part of the TRMI calculation.

Steepness (degrees)	Wetness Value (1-10)
<3.0	10
3.0 - 5.9	9
6.0 - 8.9	8
9.0 - 11.9	7
12.0 - 14.9	6
15.0 - 17.9	5
18.0 - 20.9	4
21.0 - 23.9	3
24.0 - 26.9	2
>27.0	1

Table 5: Aspect or Azimuth ° from 0 °(North, 180 ° (South) to 360 ° (North) with -1 representing flat areas. Wetness values 1-20 were applied to these aspects as shown.

Aspect °	Description	Wetness Value
-1	Neutral (flat areas)	10
0 ° (N)	Wettest (Shaded, least evaporation)	20
45 ° (NE)	Moist, receives moderate sun	16
90 ° (E)	Neutral (morning sun, less drying)	10
135 ° (SE)	Drying increases	6
180 ° (S)	Driest (maximum sun exposure)	1
225 ° (SW)	Quite dry	4
270 ° (West)	Neutral (afternoon sun, retains some moisture)	10
315 °(NW)	Moist, cooler	16
360 ° (N)	Wettest	20

Topographic Relative Moisture Index (TRMI) was calculated by summing the wetness values for aspect, slope steepness, geomophon, and TPI by summing, resulting in values between 3 and 60 (Equation 5). The TRMI values were then reclassified to a 1-10 scale using (Equation 6).

$$TRMI = (Aspect + Slope + Geomorphon + TPI) \tag{5}$$

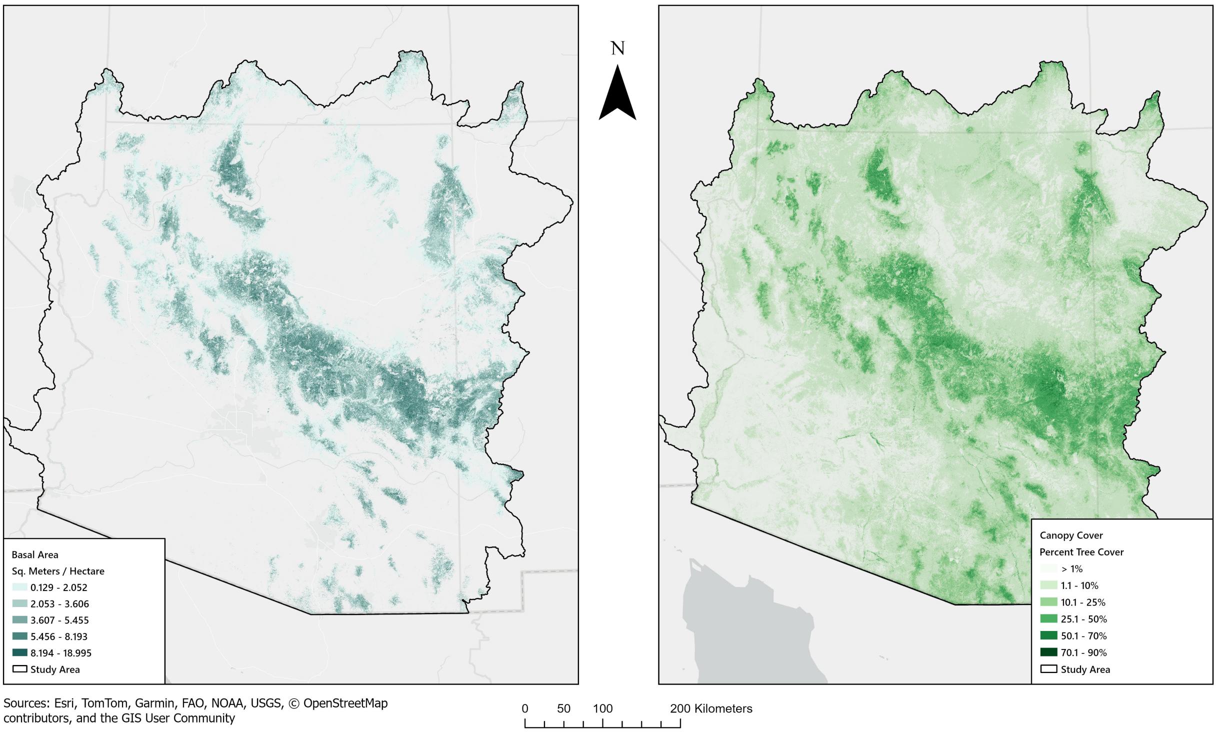

Figure 12: Canopy cover (%) from the National Landcover dataset 2021, and basal area (m^2^ ha^-1^) from Treemap 2016 are shown. These two thematic layers were combined to create the vegetation density index (VDI).

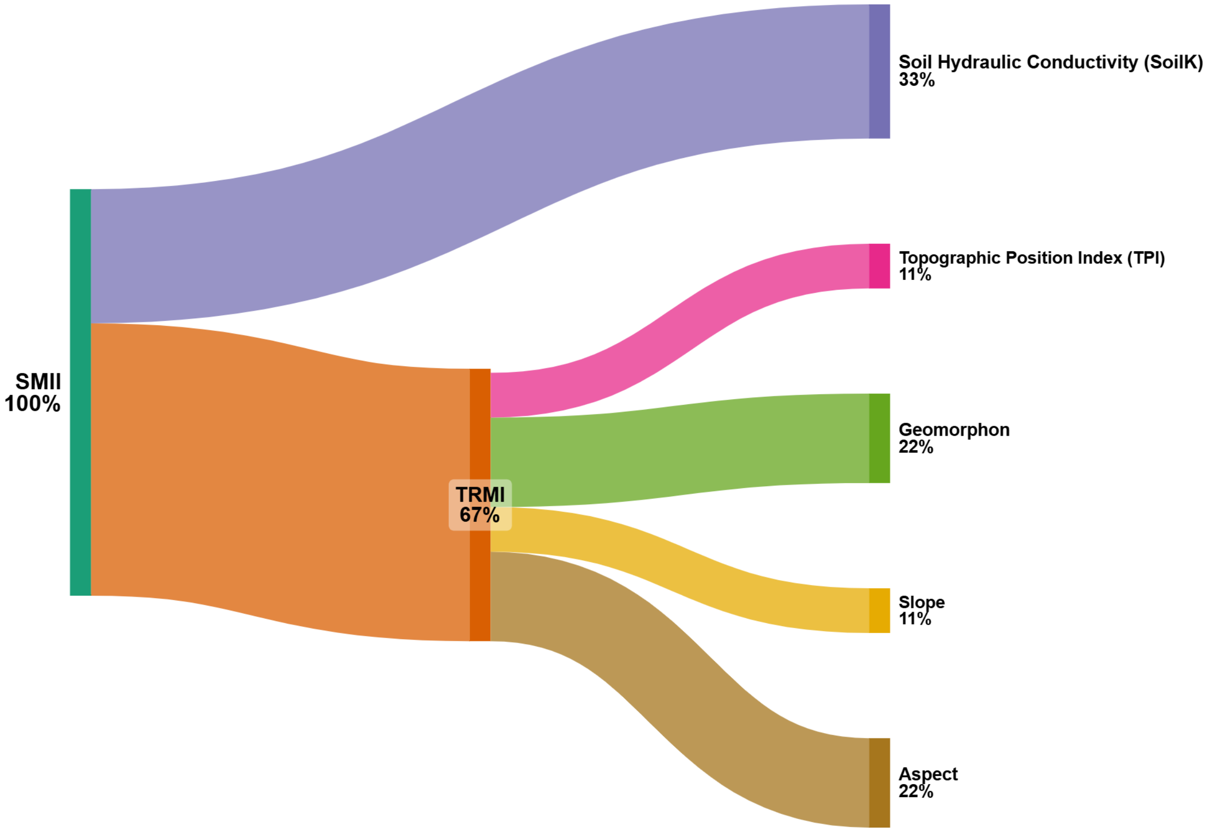

Figure 13: Sankey diagram showing the relative contributions of sTRMI and sSoilK in the Soil Moisture and Infiltration Index (SMII).

$$TRMIscaled = \frac{(TRMI - 3)}{((60 - 3) * 9)} \tag{6}$$

8.2.3. SbII

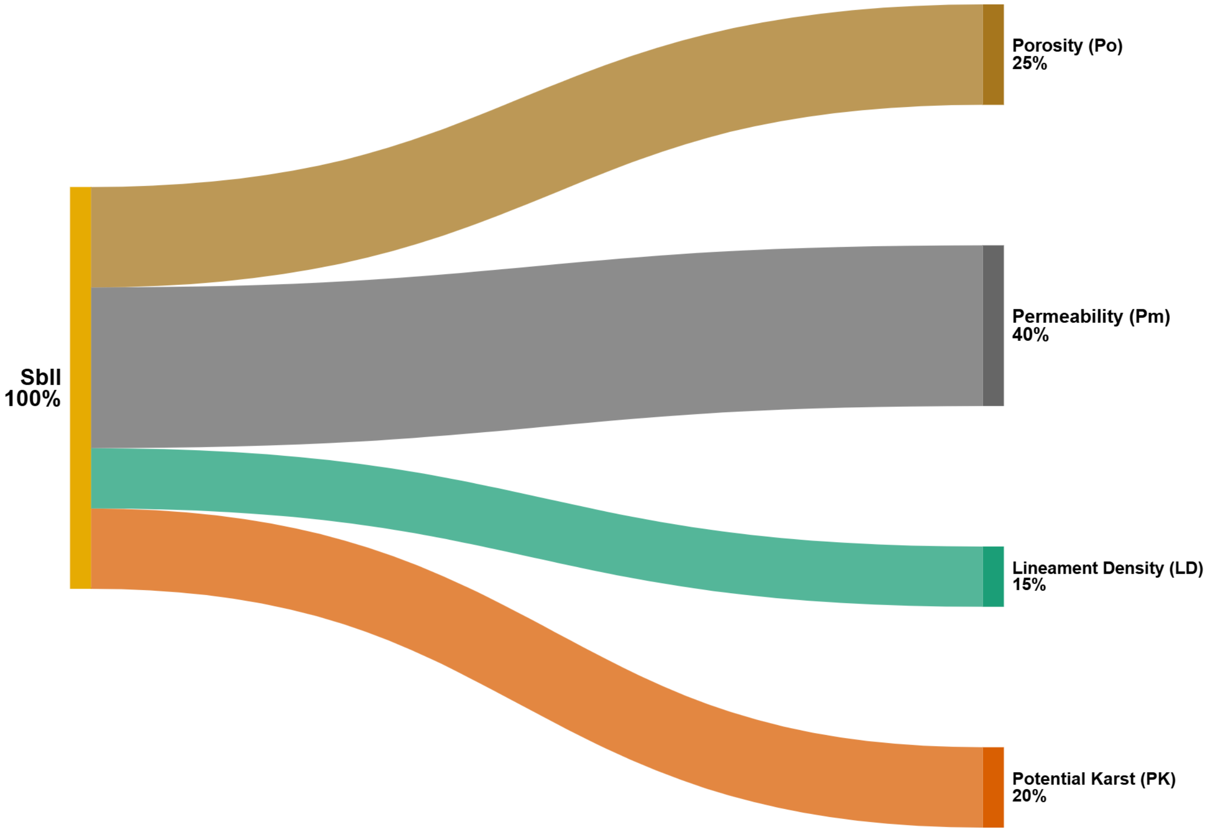

Figure 14: Sankey diagram showing the relative contributions of permeability, porosity, lineament density, and lithology (potential for karst/pseudo-karst).

Table 6: Classification and re-scaling of GLHYMPS v2 data for suitability mapping

LogK x 100 (Permeability)	Scaled Permeability (sPm)	Porosity x 100 (%)	Scaled Porosity (sPo)
-1650 to -1595	1	0 - 2	1
-1595 to -1540	2	2 - 5	2
-1540 to -1485	3	5 - 8	3
-1485 to -1430	4	8 - 10	4
-1430 to -1375	5	10 - 13	5
-1375 to -1320	6	13 - 17	6
-1320 to -1265	7	17 - 21	7
-1265 to -1210	8	21 - 24	8

LogK x 100 (Permeability)	Scaled Permeability (sPm)	Porosity x 100 (%)	Scaled Porosity (sPo)
-1210 to -1155	9	24 - 26	9
-1155 to -1052	10	26 - 28	10

8.2.3.1. LD.

Lineaments were extracted from U.S. Geologic Survey, 2019 3D Elevation Program 1-arc-second tiles using a combination of methods. First, topographic position index (TPI) which estimates neighborhood convexity and concavity was calculated using a circular neighborhood with a radius of 5m The TPI layer was then rendered as a multi-directional hillshade and exported from ArcGIS to Catalyst 3.0.2, where the LINE module was used to detect edges and link lines [109]. The default parameters for the LINE function were used (Table 7), and the resulting lineaments were brought back into ArcGIS and cleaned to remove any edge effects. A second lineament analysis was conducted as with the TPI, using a standard deviation focal statistic of elevation with a 5 m radius. This raster was also rendered, exported, and processed as before. These two rasters provided complementary sets of combined lineaments. Due to the resolution and parameters chose, man-made lineaments (roads, railways, and power-lines) were not primarily delineated by the algorithm in either analysis; however buffers around roads were randomly sampled and spot-checked to ensure man-made lineaments were not included.

Table 7: Default parameters values used to detect lineaments from the TPI and SD rasters with the LINE module of Catalyst 3.0.2. Column one shows the parameter abbreviations commonly used in the literature. Column two describes the parameters. Column three describes the units each parameter utilizes, column four shows the default values, and column five is the linear distance that the default values translate to when using a 30x30 m raster.

Parameters	Description	Units	Default Values	Distance (m)
RADI	filter radius	Pixels (30m)	10	300
GTHR	edge gradient threshold	Luminance (0-255)	100	NA
FTHR	line fitting threshold	Pixels (30m)	3	90
LTHR	curve length threshold	Pixels (30m)	30	900
ATHR	angular difference threshold	degrees	30	NA
DTHR	linking distance threshold	Pixels (30m)	20	600

8.3. Sensitivity Analysis Results

8.3.1. VDI Sensitivity Analysis

Table 8: Weight swapping VDI Results. Sensitivity analysis on vegetation density index (VDI) where variable weights were swapped. The values from the row in bold were used in the primary analysis.

Run	sBA weight	sCC weight	%>5	%>6	%>7	Mean value
VDI_0	**0.6667**	**0.3333**	**72.45**	**67.17**	**63.62**	**7.25**

Run	sBA weight	sCC weight	%>5	%>6	%>7	Mean value
VDI_1	0.3333	0.6667	78.52	73.52	63.70	7.54

Table 9: Variable Removal VDI Results.Sensitivity analysis on vegetation density index (VDI) with removal of variables One-at-a-Time (OAT) and equal weighting for the 'None condition. The values from the row in bold were used in the primary analysis.

Removed	% > 5	% > 6	% > 7	Mean Value
None	**37.46**	**33.35**	**30.86**	**7.40**
sBA	39.98	38.28	36.22	7.83
sCC	37.13	32.67	31.72	7.94

8.3.2. SMII Sensitivity Analysis

Table 10: Weight Swapping SMII results. Sensitivity analysis on soil moisture & infiltration index (SMII) where variable weights were swapped. The values from the row in bold were used in the primary analysis.

Run	sSoilK weight	sTRMI weight	%>5	%>6	%>7	Mean value
SMII_0	**0.3333**	**0.6667**	**54.32**	**20.84**	**6.90**	**5.01**
SMII_1	0.6667	0.3333	66.61	33.14	15.33	5.38

Table 11: Variable Removal SMII results. Sensitivity analysis on soil moisture & infiltration index (SMII) with removal of variables One-at-a-Time (OAT) and equal weighting for the 'None condition. The values from the row in bold were used in the primary analysis.

Removed	% > 5 % > 6 % > 7 Mean			
None	**27.00**	**12.01**	**2.58**	**5.20**
sSoilK	17.55	8.89	2.67	5.06
sTRMI	36.22	14.55	14.55	6.09

8.3.3. SbII Sensitivity Analysis

Table 12: Weight swapping SbII results. Sensitivity analysis on subsurface infiltration Index (SbII) where variable weights were swapped. The values from the row in bold were used in the primary analysis.

File	sLD	sPK	sPm	sPo	% > 5	% > 6	% > 7	Mean
SbII_0	**0.15**	**0.2**	**0.4**	**0.25**	**99.92**	**73.78**	**53.95**	**6.65**
SbII_1	0.15	0.2	0.25	0.4	99.95	58.80	0.72	5.97
SbII_2	0.15	0.4	0.2	0.25	99.97	59.41	55.62	6.58
SbII_3	0.15	0.4	0.25	0.2	99.97	59.41	54.42	6.81
SbII_4	0.15	0.25	0.2	0.4	99.92	59.37	0.72	5.95
SbII_5	0.15	0.25	0.4	0.2	99.92	74.82	54.05	6.86
SbII_6	0.2	0.15	0.4	0.25	99.93	73.78	36.96	6.55
SbII_7	0.2	0.15	0.25	0.4	99.95	40.03	0.72	5.86

File	sLD	sPK	sPm	sPo	% > 5	% > 6	% > 7	Mean
SbII_8	0.2	0.4	0.15	0.25	99.96	59.41	55.62	6.45
SbII_9	0.2	0.4	0.25	0.15	99.94	58.97	53.41	6.91
SbII_10	0.2	0.25	0.15	0.4	99.89	59.36	0.78	5.82
SbII_11	0.2	0.25	0.4	0.15	99.93	94.63	53.64	6.97
SbII_12	0.4	0.15	0.2	0.25	99.97	58.58	0.54	6.04
SbII_13	0.4	0.15	0.25	0.2	99.96	58.60	7.97	6.27
SbII_14	0.4	0.2	0.15	0.25	99.97	58.95	0.53	6.02
SbII_15	0.4	0.2	0.25	0.15	99.97	58.63	36.33	6.48
SbII_16	0.4	0.25	0.15	0.2	99.97	61.61	7.89	6.23
SbII_17	0.4	0.25	0.2	0.15	99.97	61.63	36.38	6.46
SbII_18	0.25	0.15	0.2	0.4	99.92	13.23	0.72	5.73
SbII_19	0.25	0.15	0.4	0.2	99.93	73.80	36.97	6.65
SbII_20	0.25	0.2	0.15	0.4	99.92	42.42	0.72	5.71
SbII_21	0.25	0.2	0.4	0.15	99.92	94.56	53.63	6.86
SbII_22	0.25	0.4	0.15	0.2	99.97	59.41	55.62	6.55
SbII_23	0.25	0.4	0.2	0.15	99.97	59.53	54.35	6.78

Table 13: Variable removal SbII results. Sensitivity analysis on subsurface infiltration index (SbII) with removal of variables One-at-a-Time (OAT) and equal weighting for the 'None condition. The values from the row in bold were used in the primary analysis.

Removed	% > 5	% > 6	% > 7	Mean
None	**51.84**	**29.63**	**4.14**	**6.38**
sLD	51.82	29.20	28.00	6.60
sPK5	50.91	14.58	0.37	5.88
sPm	32.28	22.01	2.53	5.75
sPo	51.83	38.63	27.67	7.28

8.3.4. Final Suitability Sensitivity Analysis

Table 14: Weight Swapping Final Suitability Results. Sensitivity analysis on overall suitability where variable weights were swapped. The values from the row in bold were used in the primary analysis.

File	Sbii	sSF	SMII	VDI	% > 5	% > 6	% > 7	Mean
Final_0	**0.2**	**0.4**	**0.2**	**0.2**	**87.41**	**63.28**	**25.75**	**6.23**
Final_1	0.2	0.2	0.4	0.2	82.07	55.72	16.32	6.00
Final_2	0.2	0.2	0.2	0.4	78.67	66.14	49.18	6.45
Final_3	0.4	0.2	0.2	0.2	90.33	67.17	27.60	6.33

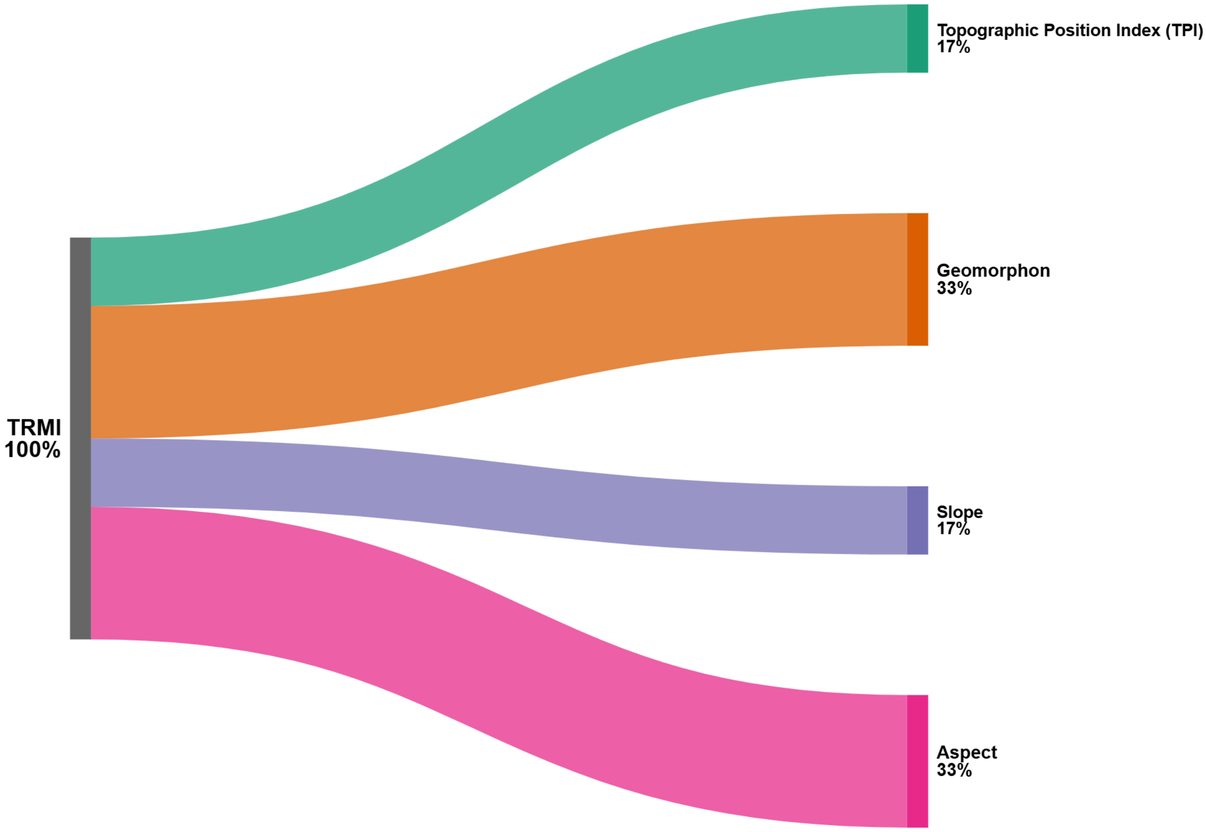

Figure 15: Topographic Relative Moisture Index (TRMI) is sum of scaled values representing site moisture potential using aspect, topographic position, geomorphon, and slope, [78]

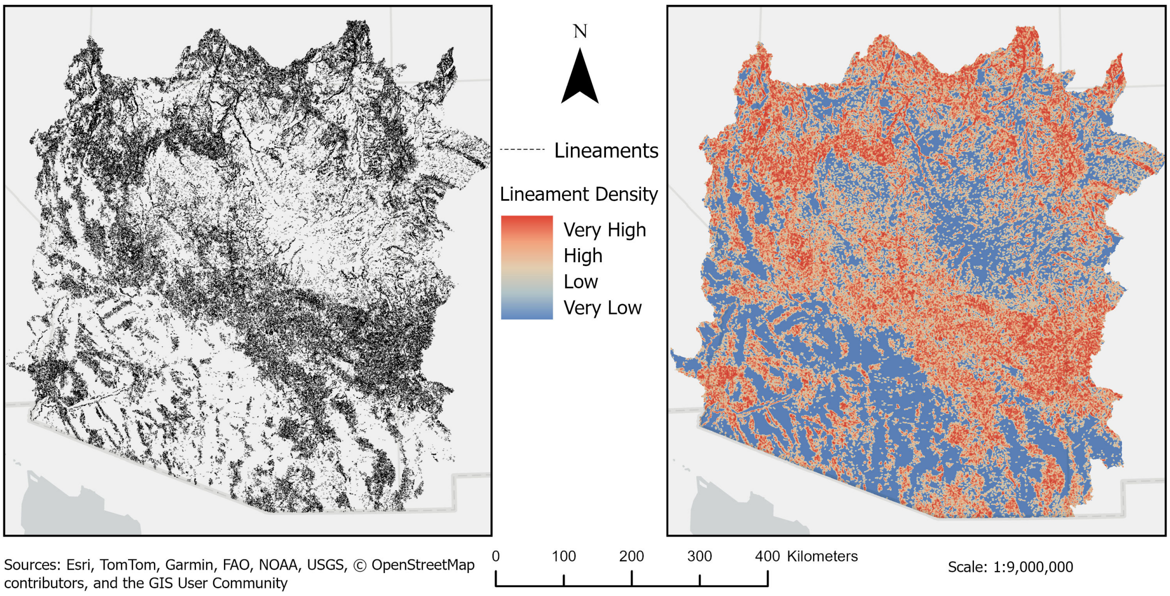

Figure 16: Lineaments (left) and Lineament Density on the right.

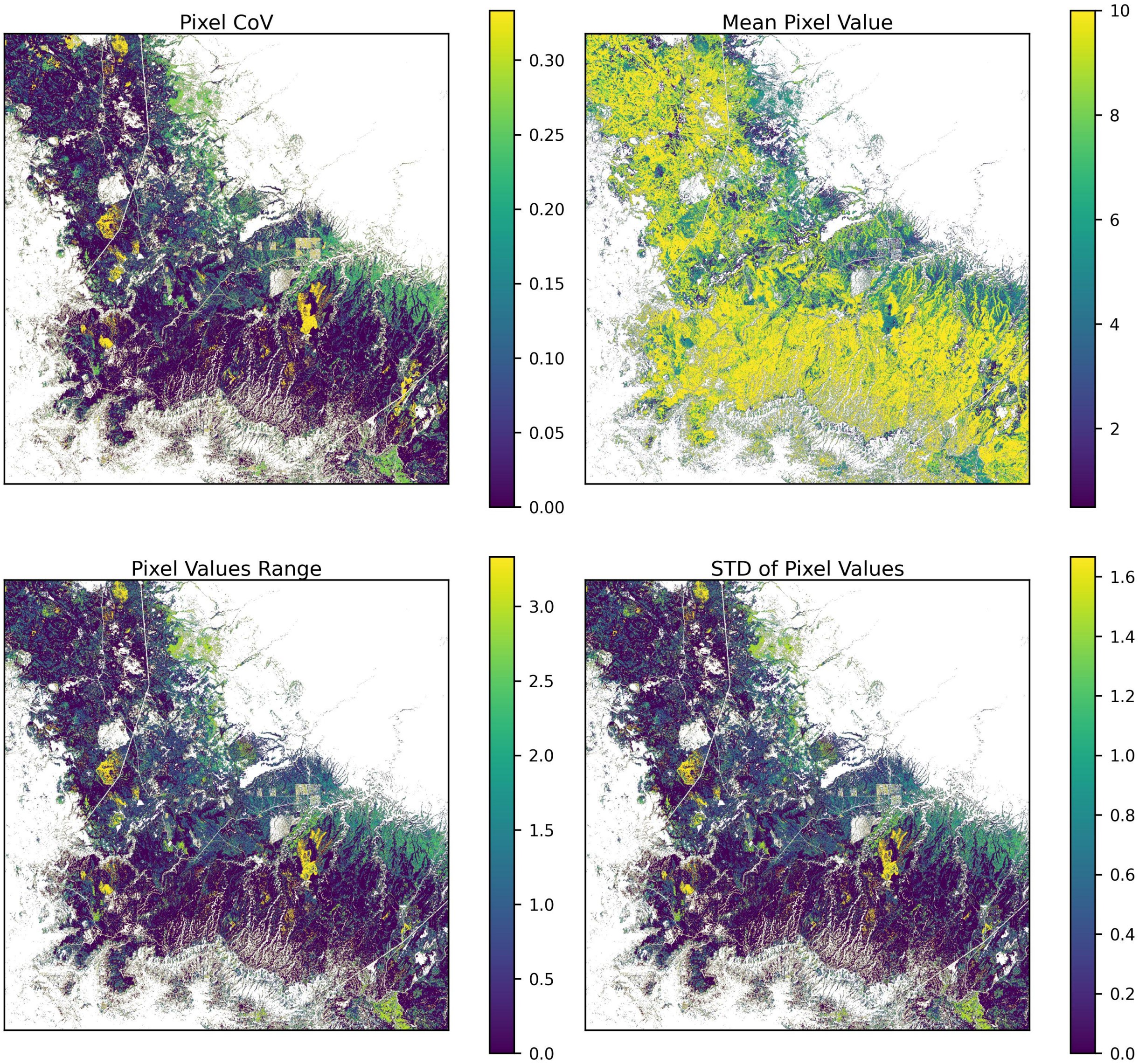

Figure 17: Pixel values across both weighting scenarios of VDI. The image shows four panels the first is pixel CoV, this is the Coefficient of Variation for each pixel in both weighting scenarios shown in the table above. Also known are Mean pixel value, the range of pixel values and the standard deviation of pixel values. There are a few spots of high variability reflected in the CoV, Range, and STD plots and these are areas with high canopy cover but relatively low basal areas, therefore we would not gain much by thinning these forests.This suggests the weighting is acting as it should for the VDI index.

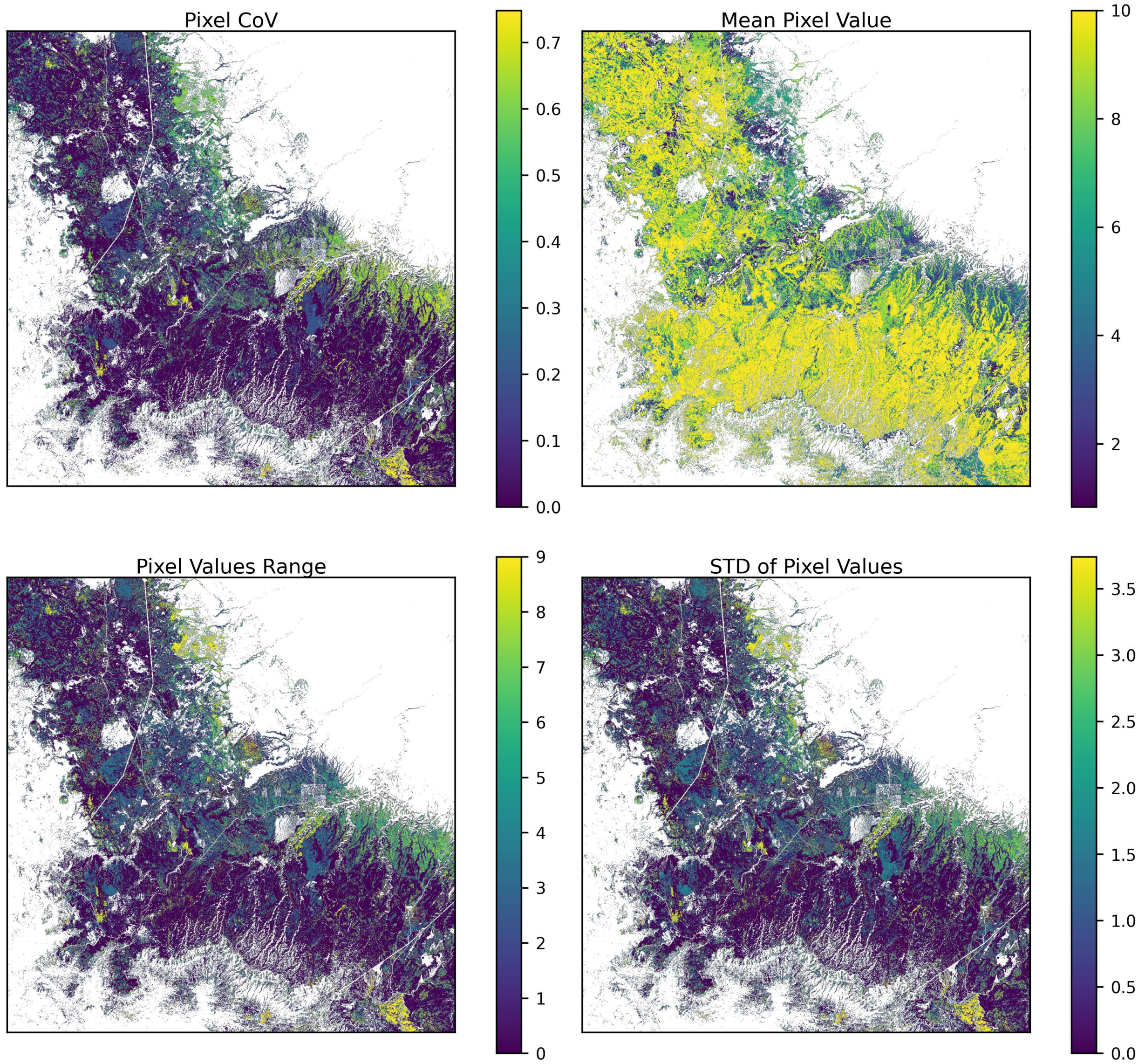

Figure 18: Pixel value variability with variable removal scenarios of VDI. The four panels show the CoV, Mean, Range, and standard deviation of pixel values across the 3 different variable removal scenarios. There is a relatively high CoV and range for areas right along the margin of the PIPO ecotone where removing either sBA or sCC significantly alters VDI values. This shows that these two variables are not redundant.

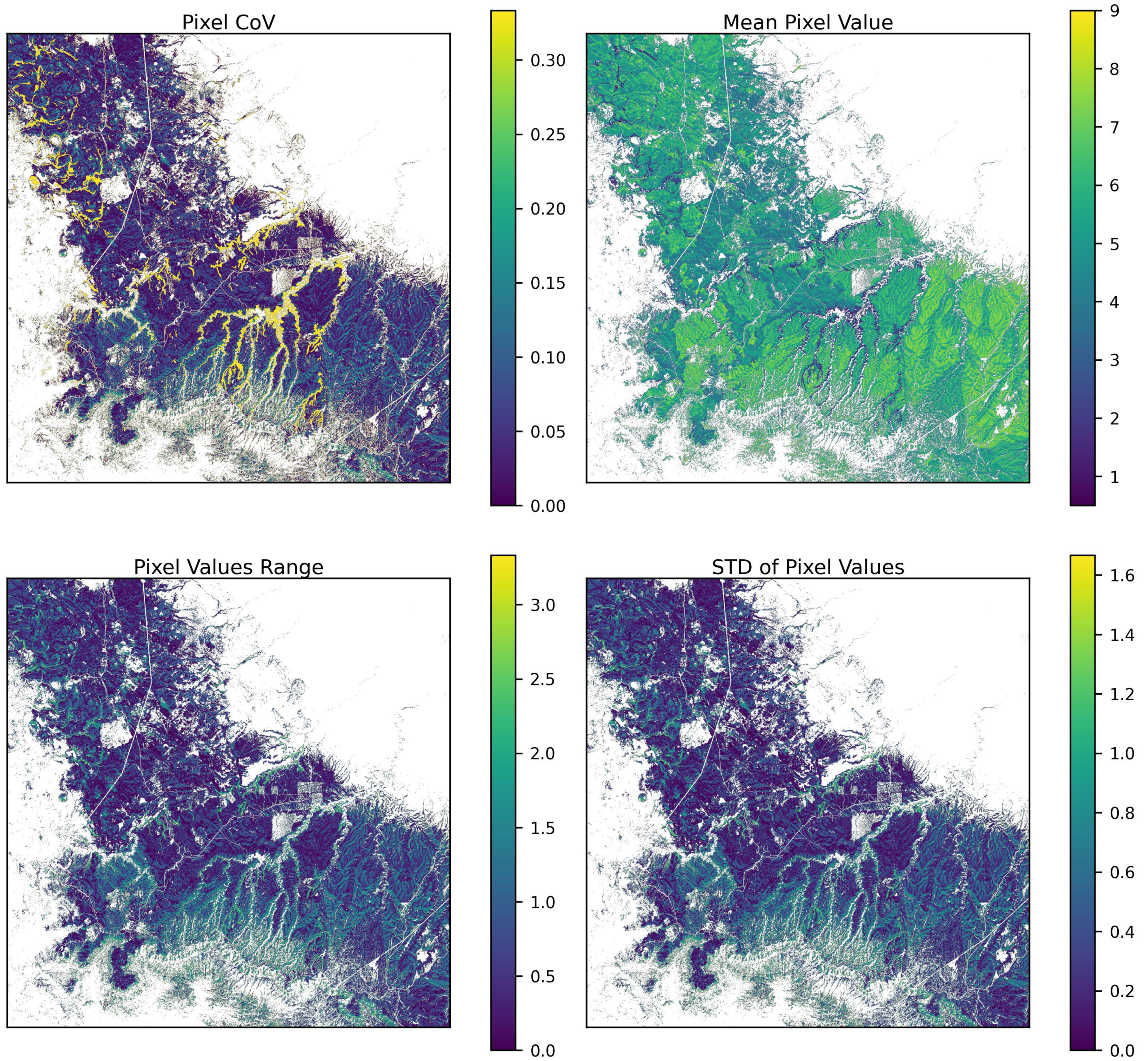

Figure 19: Pixel values across both weighting scenarios of SMII. The image shows four panels the first is pixel CoV, this is the Coefficient of Variation for each pixel in both weighting scenarios shown in the table above. Also known are Mean pixel value, the range of pixel values, and the standard deviationn of pixel values.Overall we see relatively low CoV and range maxing out at 0.32 and 3.2 respectively. mean values were lower with a higher weighting of TRMI suggesting that it is the limiting factor as shown in the table above. Which is what we indeed for TRMI to do, to limit infiltration potential to wetter areas.

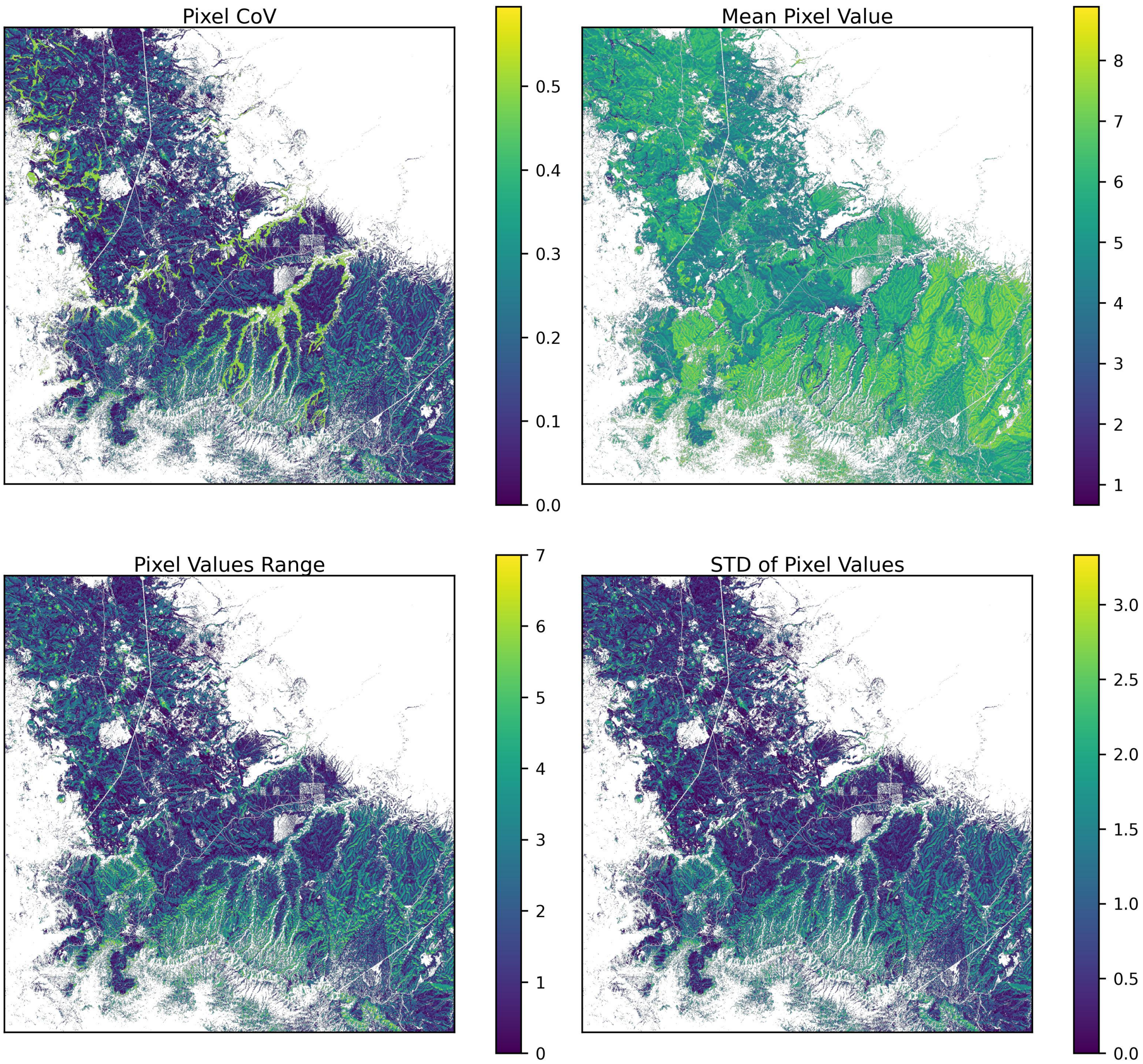

Figure 20: Pixel value variability with variable removal scenarios of SMII. Again we see that removing TRMI dramatically increases pixel values for SMII. The CoV and Range are much higher and the variation in pixel values is highest along stream channels where presumably it is wetter. We do still see that TRMI is the limiting factor in this index, which is what we intended.

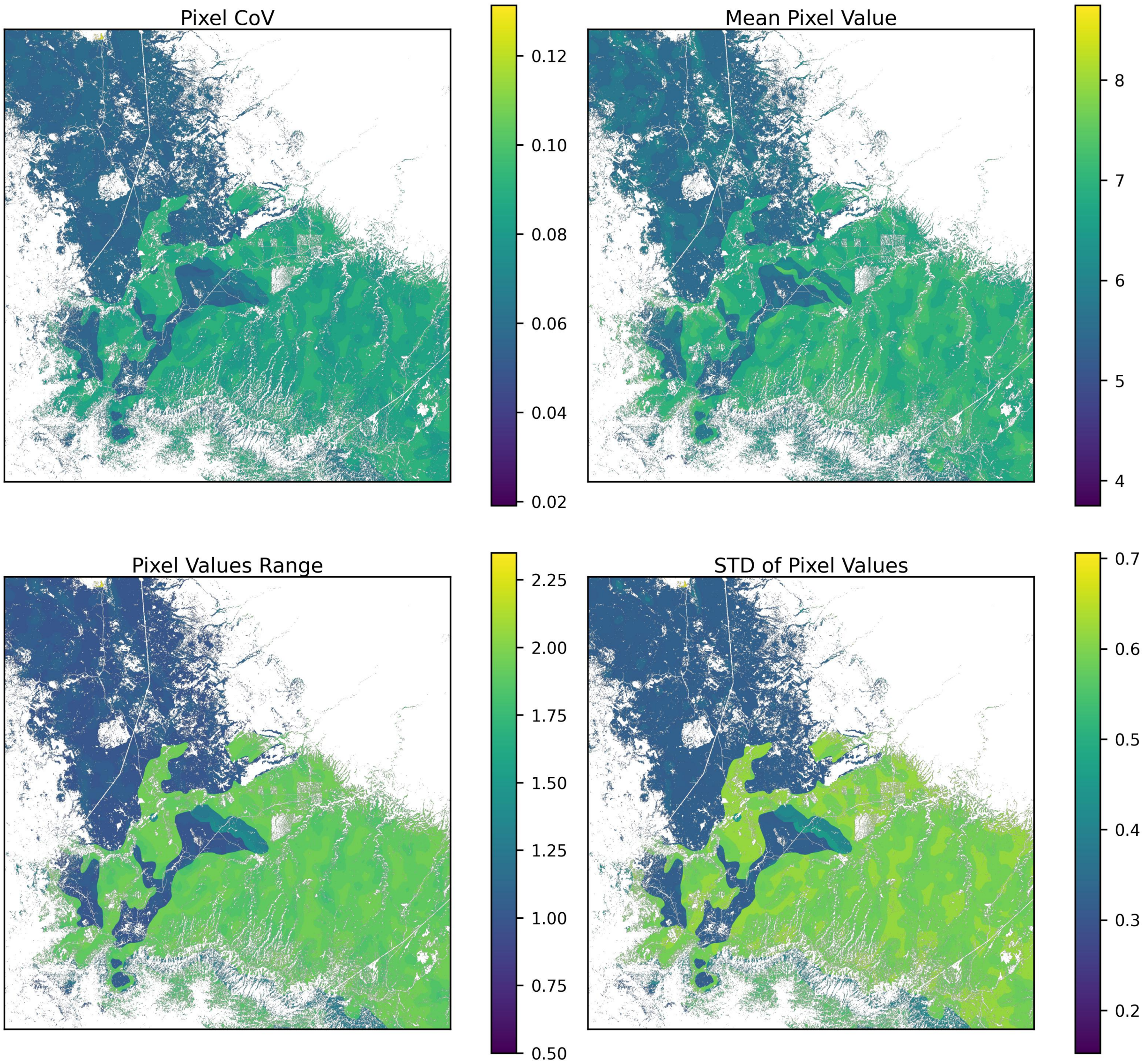

Figure 21: Pixel values across 24 weighting scenarios of SbII. We can see relatively low CoV, maxing out at around 0.13, suggesting that variable weighting does not significantly affect the value of individual pixels. However, the range of pixel values is quite large, about 2.25 in some places.

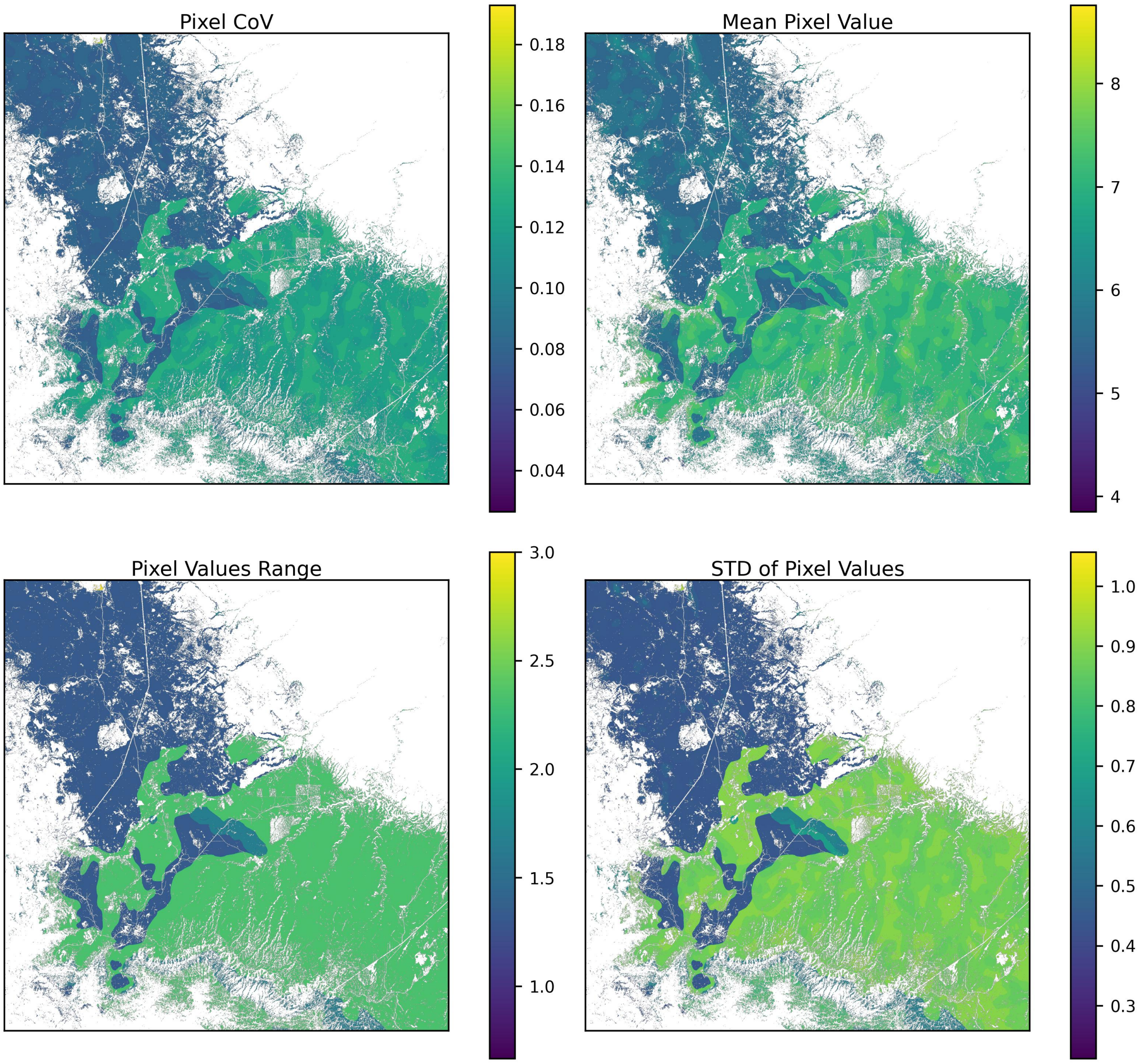

Figure 22: Pixel value variability with variable removal scenarios of SbII. Removal had a larger effect than weight swapping on overall CoV and the range of individual pixel values, but only slightly.

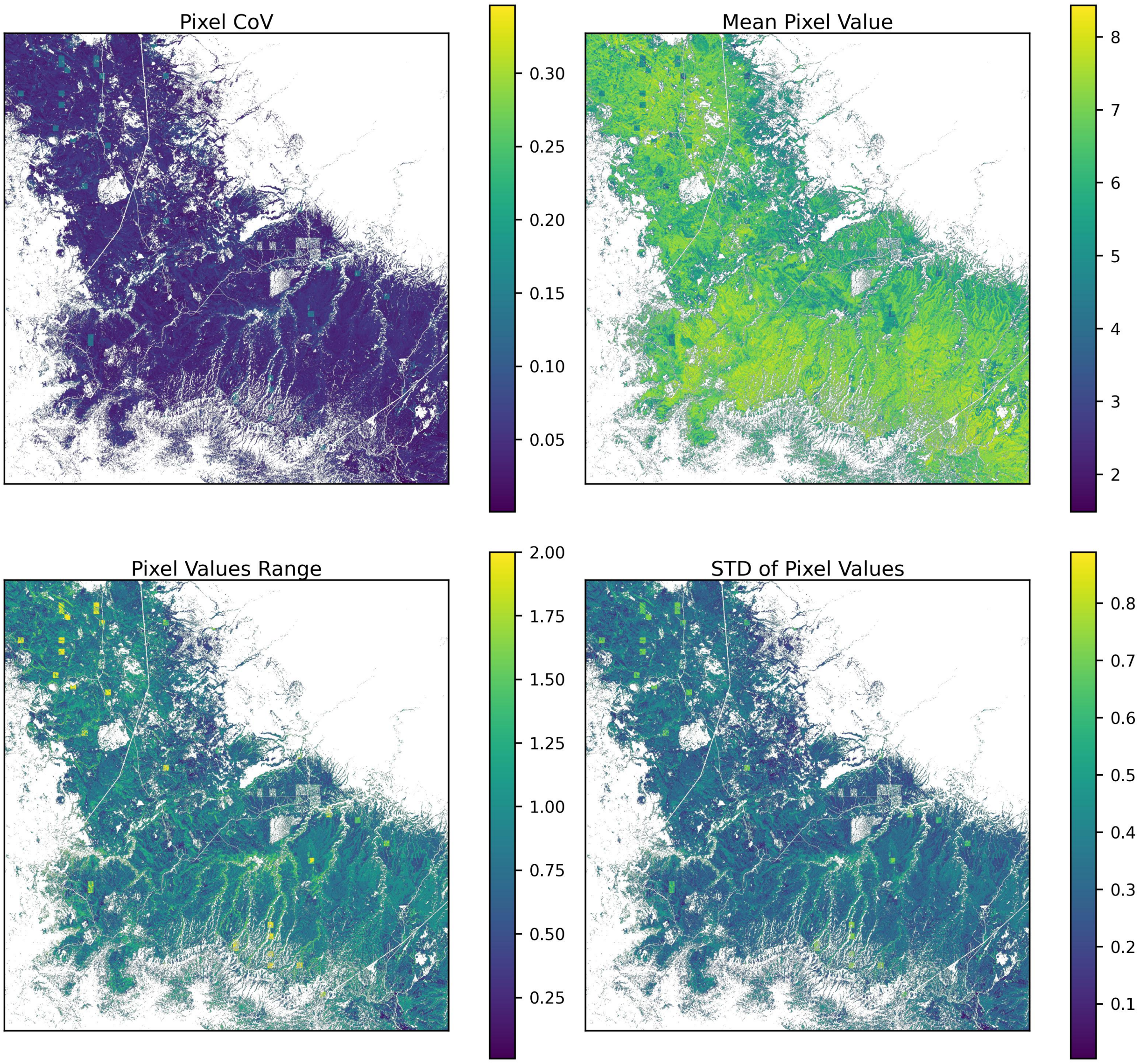

Figure 23: Pixel values across 4 weighting scenarios of Final Suitability. The CoV of the pixels tops out at about 0.32 and the maximum range of any given pixel is 2. The areas with the highest variability appear to be large square areas corresponding to the original 800m size of the sSF data. Given that sSF is the only non indexed thematic layer, it has the highest weight of any variable so this variability makes sense.

Table 15: Variable Removal Final Suitability Results. Sensitivity analysis on overall suitability with removal of variables One-at-a-Time (OAT) and equal weighting for the 'None condition. The values from the row in bold were used in the primary analysis.

Removed	$\% > 5$	$\% > 6$	$\% > 7$	Mean
None	**43.75**	**33.03**	**15.90**	**6.25**
Sbii	39.67	31.15	17.56	6.12
sSF	41.29	33.28	19.74	6.29
SMII	45.17	35.77	27.06	6.68
VDI	46.75	26.13	1.58	5.92

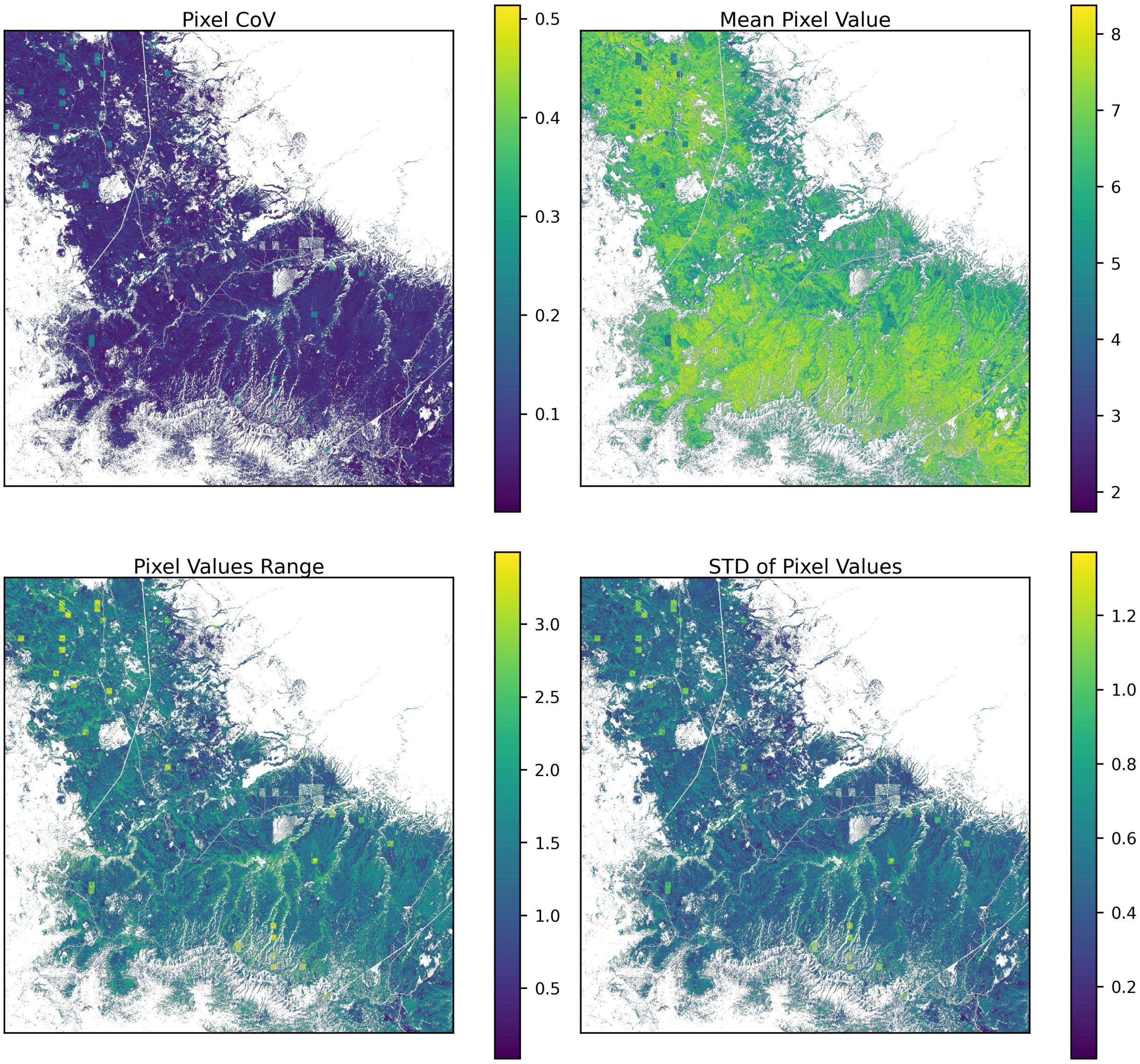

Figure 24: Pixel value variability with variable removal scenarios of Final suitability. A similar trend to what was observed in the Final Suitability swapping, a relatively high CoV of 0.5, and a maximum range for any given pixel value of 3.3. These values seem high but it also makes sense that variability would change quite a bit if these variables are capturing different (non-redundant) components of recharge suitability. The highest variability is seen in large squares again corresponding to the originally size of the sSF pixels, suggesting they are driving much of the variance.